

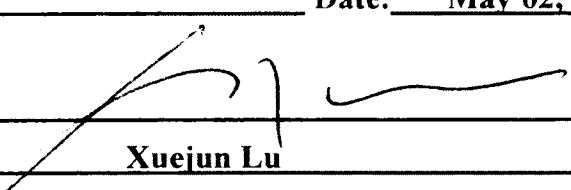
CARBON NANOTUBE GAS SENSOR CONDUCTANCE MODEL,
SENSING MECHANISM ANALYSIS, AND APPLICATIONS
IN FLEXIBLE SENSORS AND WIRELESS SENSORS

BY
YUNFENG LING

B.S. Harbin Engineering University (2004)
M.S. University of Massachusetts Lowell (2010)

SUBMITTED IN PARTIAL FULFILLMENT OF THE REQUIREMENTS
FOR THE DEGREE OF DOCTOR OF PHILOSOPHY
IN ELECTRICAL AND COMPUTER ENGINEERING
UNIVERSITY OF MASSACHUSETTS LOWELL

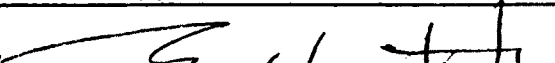
Signature of
Author:  Date: May 02, 2013

Signature of Dissertation Chair: 
Name Typed: Xuejun Lu

Signatures of Other Dissertation Committee Members

Committee Member Signature: 

Name Typed: Joel Therrien

Committee Member Signature: 

Name Typed: Tingshu Hu

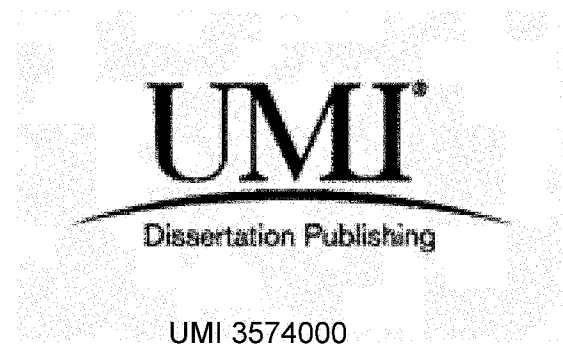
UMI Number: 3574000

All rights reserved

INFORMATION TO ALL USERS

The quality of this reproduction is dependent upon the quality of the copy submitted.

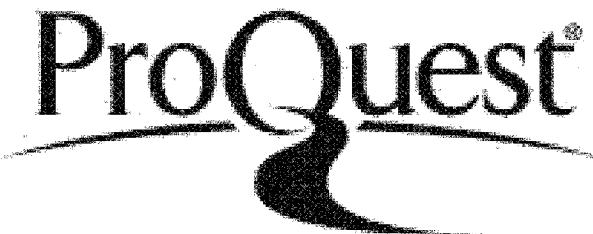
In the unlikely event that the author did not send a complete manuscript and there are missing pages, these will be noted. Also, if material had to be removed, a note will indicate the deletion.



UMI 3574000

Published by ProQuest LLC 2013. Copyright in the Dissertation held by the Author.
Microform Edition © ProQuest LLC.

All rights reserved. This work is protected against
unauthorized copying under Title 17, United States Code.



ProQuest LLC
789 East Eisenhower Parkway
P.O. Box 1346
Ann Arbor, MI 48106-1346

CARBON NANOTUBE GAS SENSOR CONDUCTANCE MODEL,
SENSING MECHANISM ANALYSIS, AND APPLICATIONS
IN FLEXIBLE SENSORS AND WIRELESS SENSORS

BY
YUNFENG LING

ABSTRACT OF A PROPOSAL SUBMITTED TO THE FACULTY OF THE
DEPARTMENT OF ELECTRICAL AND COMPUTER ENGINEERING
IN PARTIAL FULFILLMENT OF THE REQUIREMENTS

FOR THE DEGREE OF
DOCTOR OF PHILOSOPHY
ELECTRICAL ENGINEERING
UNIVERSITY OF MASSACHUSETTS LOWELL
2013

Dissertation Supervisor: Xuejun Lu, Ph.D.
Assistant Professor, Department of Electrical and Computer Engineering

ABSTRACT

In this dissertation, the electrical property dependency of carbon nanotubes (CNTs) upon the humidity and chemical gas concentration is investigated. The electrical response of single-walled carbon nanotube (SWNT) networks to different humidity levels and gas molecules of ammonia (NH_3) and nitrogen dioxide (NO_2) at different concentrations was characterized by a sensor test system. In order to exclude the effect from contact resistance, the sheet resistance of SWNT networks was measured by transfer length method. The gas molecules concentration dependence of electrical property was analyzed, and two electrical models were proposed based on carrier transportation and adsorption isotherm respectively for different gas molecules. The electrical properties of SWNT networks estimated by the models were compared with the experimental data. The results show the models agree well with the experimental data. The primary objective of the sensor model is to understand the relationship between conductance of CNT networks and gas concentration. With this understanding, the model offers a precise measurement of the gas concentration based upon the electrical property of SWNT sensor.

In addition, the mechanism of gas molecule adsorption on CNT networks is analyzed based on the conductance models. It is found that the conductance change of SWNT networks, induced by different humidity levels, is dominated by the thermal activation carrier hopping over the barriers between SWNTs. The average separation be-

tween the SWNTs increases linearly with the humidity levels. By contrast, when exposed to different NH₃ and NO₂, the conductance change is primarily determined by the charge transfer between gas molecules and CNTs. It shows that chemical molecules adsorption on the surface wall of SWNT causes the charge transfer.

Furthermore, we investigated printed flexible electronics based on SWNTs and printable SWNT-based Frequency modulation (FM) passive wireless sensor tag on a flexible substrate with enhanced sensitivity.

In this dissertation, we report a high sensitive flexible SWNT chemical gas sensor, capable of being easily fabricated. The sensor also shows good performance in linearity and flexibility. The flexible printed SWNT sensor with high sensitivity, low LOD and flexibility provides a promising solution to low-cost flexible sensor with high performance for mass production.

Last, we developed a printable SWNT-based passive FM wireless sensor tag on a flexible substrate for ammonia detection. The FM wireless sensor tag shows an enhanced sensitivity and also exhibits a high linearity between the frequency shift and the logarithm of the chemical gas concentration. The linear response allows one to precisely predict the NH₃ concentration by measuring the frequency shift of the FM wireless sensor tag. The experimental demonstration of the passive wireless sensor tag and accurate measurement of the NH₃ concentration levels indicate that the FM modulated passive wireless sensor tag is promising for power-less standalone low-level NH₃ sensing and monitoring.

ACKNOWLEDGEMENTS

First and foremost, I would like to acknowledge the kindness and the guidance of Prof. Xuejun Lu, who gave me an opportunity to continue my studies and provided the environment for me to do so. If it had not been for his tireless efforts, this journey would not have come to this point.

My gratitude also extends to Dr. Vijaya Kayastha from Brewer Science for providing the SWNT solution.

Thanks also go to my committee members, Prof. Joel Therrien and Prof. Tingshu Hu for taking time to read my proposal and providing many very helpful suggestions.

I also would like to extend my thanks to my group members for their help and suggestions during my dissertation research.

I am also grateful for the support I received from everyone in the Electrical and Computer Engineering Department, particularly the faculty members and students that volunteered their time for my experiments.

Lastly, I offer my countless thanks to my family and my wife, Yan Wang, for all the support given me during my studies.

TABLE OF CONTENTS

TABLE OF CONTENTS	vi
LIST OF TABLES	ix
LIST OF ILLUSTRATIONS	x
I INTRODUCTION	1
1 Background	1
2 Dissertation Structure.....	3
II STUDY OF CARBON NANOTUBE AND ITS APPLICATIONS....	6
1 Background	6
2 Carbon Nanotube Structure and Classifications	9
2.1 Structure of Carbon Nanotube	9
2.2 Single-walled Versus Multi-walled CNT	11
2.3 Semiconducting Versus Metallic SWNT.....	11
2.4 Purified Single-walled Carbon Nanotube	12
3 Properties of Carbon Nanotube.....	13
3.1 Electrical Property	13
3.2 Mechanical Property	15
3.3 Other Properties	16
4 CNT Gas Sensor	16
4.1 NH ₃ and NO ₂ Environmental Sensor.....	16
4.2 Humidity Sensor	17
4.3 Other Sensors.....	18
5 Mechanism of CNT Gas Sensing.....	18
6 Printed Flexible Electronics.....	19

III HUMIDITY EFFECT ON SWNT AND HUMIDITY-DEPENDENT ELECTRICAL MODEL	21
1 Background.....	21
2 CNT Network Conductance.....	22
2.1 Conductance Based on Carrier Hopping by Thermal Activation	22
2.2 Conductance Based on Tunneling Through the Inter-CNT Barriers	23
3 Experiments	24
3.1 Device Fabrication	24
3.2 Device Measurement	25
4 Results and Discussions.....	26
4.1 Contact Resistance.....	26
4.2 I-V Characteristics of the Device.....	28
4.3 Electrical Model.....	29
5 Conclusions.....	38
IV ELECTRICAL MODLE OF CNT SENSOR TO AMMONIA AND NITROGEN DIOXIDE EXPOSURE.....	40
1 Background.....	40
2 Sensing Mechanism	41
3 Experiments	42
3.1 Fabrication	42
3.2 Sheet Resistance Measurement.....	44
3.3 Conductance Model for SWNT Networks.....	45
3.4 Langmuir isotherm.....	46
4 Results and Discussions.....	47
4.1 Electrical Property Model Based Langmuir Isotherm	47
4.2 Sensing Mechanism Analysis	53
4.3 Comparison of Sensing Mechanism for NH ₃ /NO ₂ and H ₂ O	54
5 Conclusions.....	55
V FLEXIBLE CNT GAS SENSOR	56
1 Background	56

2	Sensor Fabrication	57
3	Experiments	59
4	Results and Discussions.....	59
4.1	Electrical Property Characterization.....	59
4.2	Response to Gas Exposure.....	60
4.3	Sensitivity Analysis	63
4.4	Flexibility Test.....	63
5	Conclusions.....	66
VI	WIRELESS FLEXIBLE CNT GAS SENSOR	68
1	Background.....	68
2	Flexible Printable Sensor Fabrication.....	69
2.1	CNT Sensor Design	69
2.2	Characterization of the Flexible CNT Sensor.....	71
3	Wireless Sensor Design and Wireless Test System.....	73
3.1	Wireless Sensor Design	73
3.2	Test System and Sensing Measurement.....	75
4	Results and Discussions.....	76
5	Conclusions.....	79
VII	CONCLUSIONS	81
1	Contributions.....	81
2	Suggested Areas of Further Research.....	83
3	Summary	84
VIII	REFERENCES	86

LIST OF TABLES

Table 1. T_f and T_0 parameters at different humidity levels obtained by curve fitting..... 33

LIST OF ILLUSTRATIONS

Figure 1. Images of carbon nanotubes. (a) First recorded transmission electron micrographs of carbon nanotube in low resolution, where hollow carbon fibers were first discovered by Radushkevich and Lukyanovich in 1950, from [1]. (b) Images of multiwalled carbon nanotubes observed by Iijima by transmission electron micrographs (TEM) in 1991, from [4].	7
Figure 2. Structure diagram of carbon nanotubes. (a) A single nanotube consists of a sheet of single layer of carbon atoms (graphene) and is rolled up seamlessly to a tube. The properties of the CNT is mainly determined by the roll-up vector (n, m). (b) A multiwalled carbon nanotube is composed by several rolled layers of graphene. (Images are from Ref [2]).	10
Figure 3. (a) Lattice structure of planar graphene sheet. (Images are from Ref.[3]) (b) Graphene Low Energy Band Structure. (c) Band structure of metallic SWNT. (d) Band structure of metallic SWNT. (Images are from Ref.[5])	15
Figure 4. (a) Microscopic picture of the device with two Au electrodes and SWCNT networks on Si/SiO ₂ substrate. The length L and the width of the device W are 20 μm and 500 μm , respectively; (b) AFM image of the CNT networks.	25
Figure 5. (a) Picture of the 4-channel device for R_{sh} and R_c measurement. The spacings of the channels are 5, 10, 20, and 40 μm . The width of channel is 600 μm and width of the Au electrodes is 60 μm . (b) Device resistance as a function of spacing. The intercept and the slope of the R-L curve give $2R_c$ and R_{sh}/W , respectively.	27
Figure 6. I-V characteristics of the SWCNT networks at three different humidity levels at the device temperature of 312.9K. Linear I-V curves are obtained at the bias voltage range from -2 V to 2 V, indicating ohmic contacts between the CNT networks and the Au electrodes. The slopes of the I-V characteristics give the conductance of the CNT networks.	29

Figure 7. Conductance of the device v.s. humidity levels ρ_w at different device temperature from 312.9K to 343.1K. At each temperature, the conductance decreases as the humidity level increases from 6.11 g/m ³ to 28.16 g/m ³ . The conductance increases as the device temperature increases.	30
Figure 8. $\ln \sigma$ v.s $\frac{-T_1}{T}$ plot for three different humidity levels ranging from 6.11g/m ³ to 26.77 g/m ³ . The circles, diamonds, and stars are the measured data. The solid curves the linear fittings. Very good linearities are obtained for all the humidity levels.	33
Figure 9. T_f values as a function of the humidity levels, ρ_w . The diamonds are the experimental data, and the solid line is the linear fitting curve. A good linearity between T_f and the humidity, ρ_w , was obtained with a correlation coefficient of 0.9949. The slope and the interception of the linear fitting curves are 13.58 K/g/cm ³ and 767.53 K, respectively.	35
Figure 10. Relationship between the factor A in logarithm scale and different humidity levels at device temperature 312.9K. The stars are the experimental data and the solid line is the linear curve fitting. A linear relation is obtained between $\ln(A)$ and ρ_w with a linearity of 0.9906.	37
Figure 11. Measured conductance of SWCNT networks compared with the calculated values using the model in Equation (16) at different device temperatures and humidity levels. The model agrees well with the experimental data.	38
Figure 12. (a) Picture of the device with five Au electrodes, four active channel and transparent CNT networks casted on the top of the device. (b) AFM image of the SWNT networks.....	43
Figure 13. Device resistance as a function of the device spacing. The intercept and the slope of the $R-L$ curve give $2R_c$ and R_{sh}/W , respectively.	44
Figure 14. Time response of electrical property of SWNT networks to different NH ₃ concentrations from 0 to 40.70 ppm at room temperature.....	48
Figure 15. NH ₃ sensing experiment. (a) $\frac{1}{\Delta\sigma_{sh}}$ (reciprocal of the sheet conductance change) as a function of $\frac{1}{\rho_{gas}}$ (reciprocal of NH ₃ concentration). (b) Measured	

sheet conductance of SWNT networks, compared with the calculated values by using the model in Equation (22).....	49
Figure 16. Time response of SWCNT sensor to different NO ₂ concentrations from 0 to 8.57 ppm at room temperature.	50
Figure 17. NO ₂ sensing experiment. (a) $\frac{1}{\Delta\sigma_{sh}}$ (reciprocal of the sheet conductance change) as a function of $\frac{1}{\rho_{gas}}$ (reciprocal of NO ₂ concentration). (b) Measured sheet conductance of SWNT networks, compared with the calculated values by using the model in Equation (22).....	52
Figure 18. Flexible SWNT sensor with IDE and transparent SWNT film (a) Picture of flexible SWNT sensor. (b) Interdigitated electrodes printed by using nano silver ink	58
Figure 19. <i>I-V</i> curve of the flexible CNT sensor, measured with N ₂ gas purging at the room temperature. A good linear relation is obtained, indicating ohmic contacts between SWNT networks and silver electrodes. The slope of the curve gives the value of the conductance of the flexible CNT sensor.	60
Figure 20. The response of the flexible SWNT sensor to NH ₃ gas flow with different concentrations. The squares are the measured data, and the line is linear fitting curve between ΔR/R ₀ and the chemical gas concentration in logarithmic scale..	61
Figure 21. The response of the flexible SWNT sensor to NO ₂ gas flow with different concentrations. The squares are the measured data, and the line is linear fitting curve between ΔR/R ₀ and the chemical gas concentration in logarithmic scale..	62
Figure 22. Resistance change rate dependent on the bending angle of the flexible sensor.	64
Figure 23. Comparison of the conductance change of the SWNT sensor with flat (bending angle 0°) and bent (bending angle 90°) substrate, when exposed to different NH ₃ concentrations.	65
Figure 24. Comparison of the conductance change of the SWNT sensor with flat (bending angle 0°) and bent (bending angle 90°) substrate, when exposed to different NO ₂ concentrations.	66

Figure 25. Flexible SWCNT based NH ₃ sensor. (a) Picture of the sensor with IDEs and a transparent layer of SWCNT thin film on the top of the IDEs. (b) Close-up view of the flexible SWCNT sensor. The width of the IDEs is 380 μm , the separation between two IDE fingers is 180 μm , and the length of the IDE is 1400 μm	70
Figure 26. Relative resistance changes $\Delta R/R_0$ vs log [NH ₃] curve. The resistance of the sensor increases with the concentration of the NH ₃ gas due to the electron donation from the NH ₃ molecules to the SWCNT networks. The squares are measurement data and the line is the linear fitting curve. A good linear relationship is obtained between the resistance of the sensor and the log [NH ₃].	72
Figure 27. Circuit diagram of the passive FM wireless sensor tag. It consists of an RF antenna, a rectifier, a modulator, a ring oscillator, and the flexible SWNT gas sensor.	74
Figure 28. Diagram of the test system for the wireless device.	76
Figure 29. (a) Output waveforms of the ring oscillation of wireless sensor tag when exposed to different NH ₃ concentration levels of NH ₃ of 2.85 ppm and 23.7 ppm, corresponding to the CNT sensor resistances of $R=1.45 \text{ k}\Omega$ and $R=1.63 \text{ k}\Omega$, respectively. The frequencies of the ring oscillator signals are 33.23 kHz and 31.97 kHz, respectively. (b) Spectra of the received signals by the reader. The frequencies agree well with the output waveforms of the ring oscillator, indicating the effectiveness of the FM modulation and the wireless sensing configuration.	77
Figure 30 Linearity analysis of the wireless sensor tag. The circles and diamonds are the experimental data and the solid line is the linear fitting curve. Oscillation frequencies vs the resistances of the CNT sensor. A good linearity ($R^2=0.996$) is obtained between the sensor resistance and the oscillation frequency.	78
Figure 31. Linearity analysis of the wireless sensor tag. The circles and diamonds are the experimental data and the solid line is the linear fitting curve. Linear relation between the log [NH ₃] curve and the oscillation frequency with a linear correlation (R^2) of 0.988.	79

I INTRODUCTION

1 **Background**

Since its discovery, Carbon nanotubes (CNTs) have been extensively studied recently. Due to their unique electronic, mechanical and other properties, CNTs have shown great promise in various applications ranging from nanoelectronics [6, 7] to chemical sensor technology [8, 9]. One-dimension structure with diameter in size of nanometer scale, resulting in quantum effect in CNT, makes intrinsic properties extremely sensitive to external environmental change. In addition, CNT also possesses exceptionally high surface to volume ratio. These characteristics lead the CNT a strong and promising candidate for gas sensor with high sensitivity.

Meanwhile, as the development of nanotechnology, it offers human-beings capable of manipulating matter on an atomic and molecular scale [10]. Nanotechnology, which is defined by size, is naturally very broad, including fields of science as diverse as semiconductor physics [11], material science [12-17], microfabrication [18-20], chemistry [21], molecular biology [22-27], nanometrology [28-30], etc. Its development facilitates the study and research for CNTs.

Also, the demand for various gas sensors from human-being society has been increasing in many aspects of our life, such as in public security [31], food quality control, industrial emission monitoring and control [32, 33], environmental pollution analysis [34],

and bio-hazard monitoring [35-37]. The sensor technology is of great importance to human-being, not only protecting our safety and improving the quality of our daily life but also benefitting the industry development. Therefore, with promising sensing properties, CNTs have aroused a great deal of attention for gas sensor applications.

Many groups have designed various gas sensors using CNTs as an active material, and investigated the variation of the conductance of the CNT networks with the gas molecules adsorption, such as NH₃, NO₂, H₂O, etc [7, 8]. However, the electrical property model of CNT networks and its dependence on the gas concentration have not been investigated, and mechanism of the sensing behavior is not clear yet.

In this dissertation, we investigated the electrical property dependency of SWNT networks upon the humidity and chemical gas concentration. The electrical response of SWNT networks to different humidity level and gas molecules of NH₃ and NO₂ at different concentrations was characterized by a sensor test system. The gas molecules concentration dependence of electrical property was analyzed, and two electrical sensor models were proposed based on carrier transportation and adsorption isotherm respectively for different gas molecules. The electrical property models of SWNT networks were compared with the experimental data. The results show the models agree well with the experimental data. The primary objective of the sensor model is to understand the relationship between conductance of CNT networks and gas concentration. With this understanding, the model offers a precise measurement of the gas concentration based upon the electrical property of SWNT sensor. Moreover, the mechanism of gas molecule adsorption on CNT networks is analyzed based on the models.

In addition, we investigated printed flexible electronics based on SWNTs and printable SWNT-based FM passive wireless sensor tag on a flexible substrate with enhanced sensitivity [38]. A high sensitive flexible SWNT chemical gas sensor, capable of being easily fabricated, is reported. The flexible printed SWNT sensor with high sensitivity, low LOD and flexibility provides a promising solution to low-cost flexible sensor with high performance for mass production. Last, we developed a printable SWNT-based passive FM wireless sensor tag on a flexible substrate. The experimental demonstration of the passive wireless sensor tag and accurate measurement of the NH₃ concentration levels indicate that the FM modulated passive wireless sensor tag is promising for powerless standalone low-level NH₃ sensing and monitoring.

2 Dissertation Structure

In this dissertation, the electrical property of SWNT has been studied under different gas concentration, and flexible SWNT gas sensor and wireless flexible SWNT sensor are also investigated as SWNT applications. The dissertation is organized as following:

Chapter II: The history and background of carbon nanotubes will be presented together with CNT properties, applications in gas sensor, and also with reviews on the CNT gas sensing mechanism. An introduction of flexible CNT sensors and wireless CNT sensors will also be discussed.

Chapter III: In this chapter, we investigate the conductance of SWNT networks at different humidity levels and various device temperatures. The carrier transport processes are analyzed by performing a temperature-dependent conductance study. It is found that the conductance of the SWNT networks is dominated by the thermal activation

carrier hopping over the barriers between CNTs. The average separation between the SWNTs is found to vary linearly with the humidity levels. The humidity-dependent conductance of the SWNT network is modeled and compared with the experimental data. The model agrees well with the experimental data.

Chapter IV: In this chapter, we present a study on the electrical property model of a single-walled carbon nanotube chemical gas sensor of NH₃ and NO₂. First, the electrical response of SWNT networks of the sensor to chemical gas flow with different concentrations is characterized. The ammonia concentration-dependent conductance is further modeled based on Langmuir adsorption isotherm. The experimental data agrees well with the model with a high correlation coefficient. Our experimental result provides a method of measuring of NH₃ and NO₂ concentration based upon the electrical property of CNT sensor. Last, the mechanism of ammonia adsorption on CNT networks is analyzed. It is found that the CNT sensing mechanism in this study is dominantly determined by the charge transfer between CNTs and chemical gas molecules adsorbed on CNTs.

Chapter V: In this chapter, we report a high sensitive flexible gas sensor based on single-walled carbon nanotube for sensing toxic gas molecules of NH₃ and NO₂. The sensor is capable of being easily fabricated. Due to the high purity of the semiconducting SWNT, the flexible sensor obtains a high sensitivity, 1.32%/ppm for NH₃ detection, and 6.17%/ppm for NO₂. The lowest detectable concentrations are 2.85 ppm for NH₃, and 659 ppb for NO₂ respectively, way below the required threshold limit value. Additionally, the sensor not only exhibits a high linearity of the response to gas exposure, but also shows good performance in the reproducibility and flexibility. Such a flexible printed SWNT sensor with a high sensitivity, low detectable concentration, and good reproduc-

bility provides a promising solution to low-cost flexible sensor with high performance for mass production

Chapter VI: In this chapter, we investigate a frequency-modulated (FM) passive wireless sensor tag for ammonia sensing. The passive wireless sensor tag consists of a single-walled carbon nanotube network based NH₃ sensor, a radio frequency (RF) antenna, a ring oscillator, and other supporting circuits. The SWNT network based NH₃ sensor is fabricated on a flexible plastic substrate through printable processes. The printable SWNT based NH₃ sensor shows an enhanced sensitivity of 0.76% per parts per million (ppm) primarily due to the large surface area of the SWNT network. The sensor also exhibits a high linearity between the resistance of the sensor and the logarithm of the NH₃ concentration. A simple frequency-modulated circuit is designed to convert the resistance change of the sensor to the oscillating frequency shift of the circuit. By properly designing the circuit, we have obtained a linear response between the frequency shift and the logarithm of the NH₃ concentration. The linear response allows one to precisely predict the NH₃ concentration by measuring the frequency shift of the FM wireless sensor tag. Such FM modulated passive wireless sensor tag with linear response and enhanced sensitivity is promising for power-less standalone low-level NH₃ sensing and monitoring with high accuracy.

Chapter VII: In this chapter, the contributions of the dissertation are summarized and suggested areas of further research future wok are discussed.

II STUDY OF CARBON NANOTUBE AND ITS APPLICATIONS

1 **Background**

The existence of carbon nanotubes was recorded by transmission electron microscope (TEM) micrographs (as shown in Figure 1 (a)), showing hollow graphitic carbon fibers with 50 nm in diameter [1], and the first paper on carbon nanotubes published by Radushkevich in the Soviet Journal of Physical Chemistry in 1952 [39].

However, without the capability of reliable production and characterization for carbon nanotube, little attention had been paid in academic or industrial fields until 1991. Multi-walled Carbon nanotube (as shown in Figure 1 (b))was rediscovered by Sumio Iijima, when he was studying the byproducts of C₆₀ fullerenes, which were synthesized by arc discharge method with high resolution transmission electron microscopy in 1991 [4]. Then, single-walled carbon nanotube, which is much more significant due to its unique semiconducting property, was discovered by Iijima and Ichihashi at NEC [40] and Bethune et. al. at IBM [41] independently in the same year of 1993. In the last decades, following these pioneering researches, carbon nanotubes have been extensively studied in academic and industrial areas, and various applications have been proposed and developed in different fields ranging from nanoelectronics [7], bio-sensor technology [42], to gas sensor technology [43].

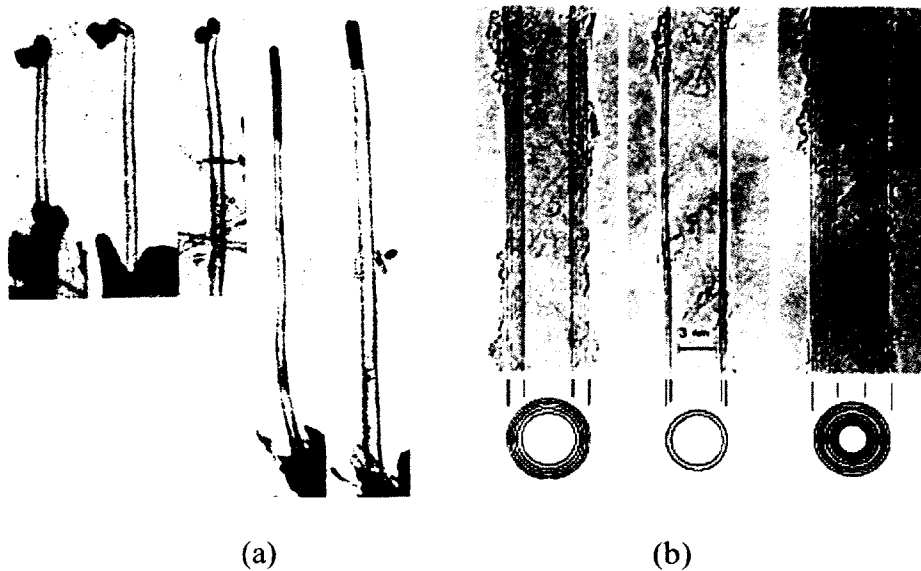


Figure 1. Images of carbon nanotubes. (a) First recorded transmission electron micrographs of carbon nanotube in low resolution, where hollow carbon fibers were first discovered by Radushkevich and Lukyanovich in 1950, from [1]. (b) Images of multiwalled carbon nanotubes observed by Iijima by transmission electron micrographs (TEM) in 1991, from [4].

Among vast applications of the carbon nanotube, gas sensor is playing a significant role. With the development of the nanotechnology, state-of-the-art sensor is capable of detecting gas molecules in the environment with good sensing performance. Especially, owing to miniature and portable sensors, the gas sensors are widely employed in industrial emission monitoring, environmental pollution analysis, public security, and control, agriculture and medical diagnosis.

A gas sensor can be defined as a device, capable of varying its properties (electrical, chemical, optical, etc.) upon exposure to chemical gaseous molecules in the local chemical environment. The change in these properties is usually converted into an elec-

trical signal to detect the analytes by an electrical device/system. Generally, a practical gas sensor, with certain constraints of size, weight, cost etc., is expected to respond to chemical gas with fast response and acceptable precision within certain ambient and process conditions (i.e., within the required range over an acceptable lifetime)

Carbon nanotubes have attracted much attention for various potential applications, particular for nanoscale sensors. Two main characteristics indicate carbon nanotube as a promising candidate for extremely sensitive gas sensors. First, the ‘quantum nature’ makes the carbon nanotubes possess the extremely high sensitivity of intrinsic properties to small external perturbations due to its ‘quantum nature’ because of its one-dimensional systems in nanometer size. Second, there is huge active surface area on carbon nanotube.

Currently, gas sensors have been extensively employed in medical analysis, toxic gas monitoring, automobile combustion control, energy and drying operations markets. Additionally, there is increasing demand for gas sensors in the emerging markets, such as consumer products, automobiles, defense, food processing, wastewater treatment, etc. Market for gas sensors, detectors, and analyzers is expected to grow further in the future. Legislation and public concerns regarding monitoring of gas leaks and emissions stimulate market growth. The increasing awareness on safety among end users leads to a greater demand for gas sensors and detectors. Increasing enforcement of the occupational health and safety regulations and government bodies is an important driver for the sales of gas sensors, detectors, and analyzers. With extensive CNT applications in gas sensor, an increase of CNT gas sensor market will be expected, with the advantage in sensitivity, miniature size, and low cost.

2 Carbon Nanotube Structure and Classifications

2.1 Structure of Carbon Nanotube

There are several methods proposed to classify carbon nanotubes. Among them the most common approach to categorize nanotubes is according to the structure of the CNT, particularly the number of walls in the tube. Primarily, CNTs are divided in two different types, determined by the number of the walls of the nanotube.

A SWNT consists of a sheet of single layer of carbon atoms (graphene) and is rolled up seamlessly to a cylinder, as shown in Figure 3Figure 2(a). The properties of the SWNT are mainly determined by the roll-up vector (chirality) (n, m). Depending on the chirality, there are three different structures for SWNTs, including armchair ($n = m$), zig-zag ($n = 0$ or $m = 0$), and chiral (any other n and m).

A multi-walled carbon nanotube is composed by several rolled layers of graphene, as shown in Figure 3Figure 2(b). There are two structural models of multi-walled nanotubes, including Russian Doll model and Parchmen model. The individual shells of MWNT can be described as SWNTs, which could be either metallic or semiconducting. However, due to statistical probability and restrictions on the relative diameters of the individual tubes, the whole MWNT usually behaves as a zero-gap metal.

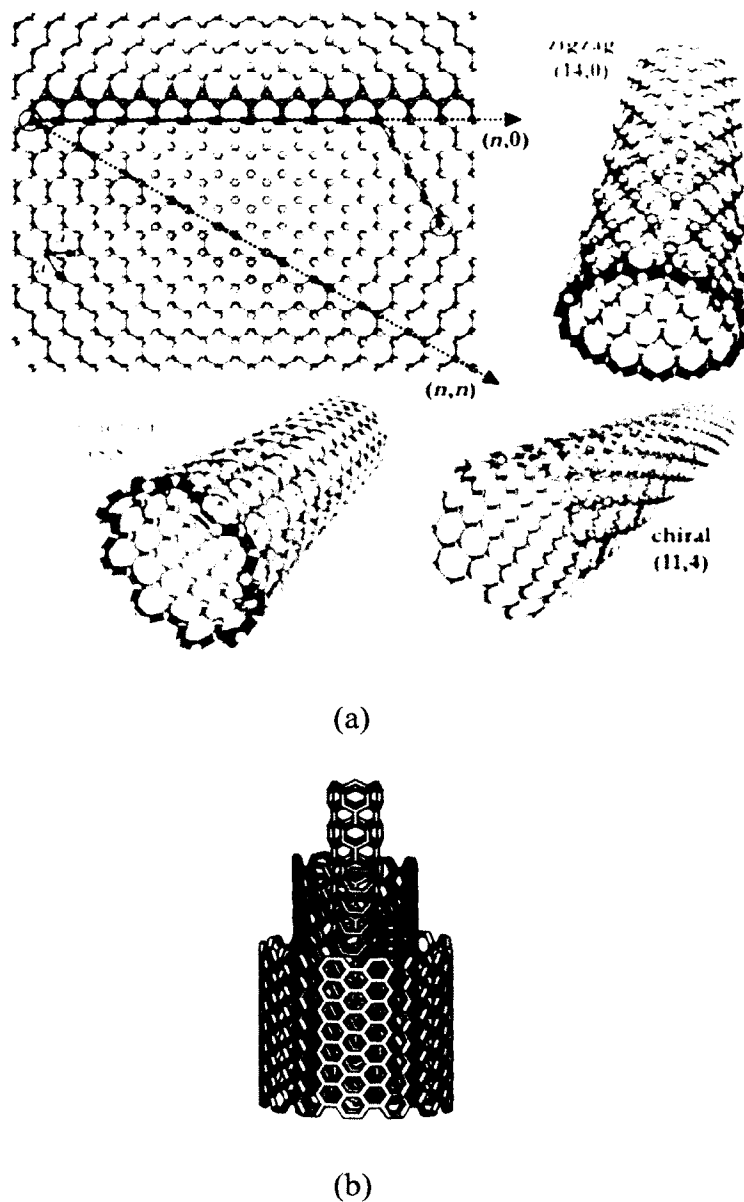


Figure 2. Structure diagram of carbon nanotubes. (a) A single nanotube consists of a sheet of single layer of carbon atoms (graphene) and is rolled up seamlessly to a tube. The properties of the CNT is mainly determined by the roll-up vector (n,m) . (b) A multiwalled carbon nanotube is composed by several rolled layers of graphene. (Images are from Ref [2])

2.2 Single-walled Versus Multi-walled CNT

As an extremely promising class of novel materials, single-walled carbon nanotubes have been much more extensively studies than multi-walled carbon tubes, especially as a new electrical material, due to many factors.

First, the quantum effect, resulting from the size in nanometer scale of the nanotube, primarily determines the properties of the material, especially electrical properties. SWNT has lower size in diameter, which is around 1.5 nm in average for many electrical applications. The nano-scale size causes direct band gap in some nanotubes, leading into semi-conductive behavior of the SWNT. By contrast, MWNT is larger in diameter due to its multi-walled structure. The quantum effect is suppressed by the relatively large size of the structure. Therefore, for some electrical applications, MWNTs perform poorly due to insufficient band gap.

Secondly, the defects and impurities play an important role in determining the performance of CNTs. From its definition of MWNT, nanotubes with multiple concentric layers of walls are classified as MWNT. These walls inherently contain more defects and impurities to some extent than a SWNT. In general, SWNTs have fewer defects and impurities. Moreover, SWNTs have a higher degree of crystallinity than MWNTs. Therefore, varieties of applications based on SWNTs obtain superior performance to the ones with MWNTs.

2.3 Semiconducting Versus Metallic SWNT

Experiments and theory have shown that SWNTs behave as a metallic conductor or as direct band gap semiconductor, indicating SWNTs exist in both metallic and semiconducting forms. Further investigations found that this property depends on chirality and

diameter of SWNTs. The relationship between the chirality and electrical property will be discussed in details in the following section.

Both metallic and semiconducting SWNTs have been found to possess superior electrical characteristics to the best electronic materials available on the market to some extent.

One-dimensional structure with nanometer scale in diameter enables ballistic electronic transport along the nanotube axis without scattering due to the quantum effect. Thus, the CNT can carry high current density without heat dissipation. Theoretically, metallic SWNT is capable of conducting a current density 1000 times higher than that of metals (i.e. copper) [5]. Therefore, metallic SWNTs have been proposed as advanced interconnects in some applications for high current density, such as electrodes for Li-ion battery, transparent display, photovoltaic device, etc.

While, semiconducting SWNTs offer a promising ultrasmall semiconductor, providing great potential for modern device applications, such as field effect transistor, single-electron transistor, nanoscale p-n junction, etc. Also, it has shown that for CNT chemical sensors based on chemiresistor and back-gated chemical field effect transistor (ChemFET), semiconducting SWNTs offer higher sensitivity comparing with metallic SWNTs in various chemical environment, due to more sensitive shift of the Fermi level in semiconducting SWNTs [44].

2.4 Purified Single-walled Carbon Nanotube

The main obstacle in designing SWNT electrical device with high performance is the impurities in CNTs networks or bundles. These impurities are usually the byproducts from CNT synthesis, such as metal particles, amorphous carbon, and carbon nanoparti-

cles. They are adsorbed on the outer surface of SWNTs or tightly entangled with SWNTs, causing a serious impediment for their properties. In order to improve the CNT device quality, for most electronic applications, SWNTs have to be pure and highly enriched with either metallic or semiconducting SWNT according to specific application. By removing the impurities from CNTs, purified and unsorted SWNTs offer superior electrical properties compared to untreated CNTs.

In this dissertation, we mainly exploit the semiconducting property of highly purified SWNTs to develop gas sensors with high performance.

3 Properties of Carbon Nanotube

CNTs have many exceptional properties, therefore attracting researchers in variety of disciplines into intensive studies. The impressive properties in aspects of electrical mechanical, and others, along with their potential applications, are reviewed in this section.

3.1 Electrical Property

SWNTs can be either metals or semiconductors, and the property is determined by its special structure and material.

SWNT is composed of a sheet of graphene, a single atomic layer of graphite. As shown in Figure 3 (a), graphene consists of sp^2 bonded carbon atoms in a 2D honeycomb pattern. Because of its unique band structure, which is described as Brillouin zone (as seen in Figure 3 (b)), the graphene behaves as a zero-bandgap semiconductor. It is metallic in some directions, and semiconducting in others. In a SWNT, rolled up by a sheet of graphene, the momentum of electrons is quantized when they are moving around the circumference of the SWNT. Depending on how the allowed momentum states compared

with the preferred directions for conduction, SWNT is either one dimensional metals or semiconductors [45, 46].

CNT is a new nano-material with amazing electrical properties, dependent on the tube diameter and chiral vector (n, m). When n is $n = m$ (armchair nanotubes) or $n = m+3N$ (N is an integer), the nanotubes are supposed to be metallic CNT (as shown in Figure 3(c)). In other cases, CNT is semiconducting material with different energy gaps (as shown in Figure 3 (d)), determined by the diameter of the tube, inversely proportional to the tube diameter. The band gap is estimated to be $Eg = 0.9 \text{ eV}/d [\text{nm}]$, where d is the diameter of SWNT.

Therefore, SWNTs can be either metals or semiconductors, depending on how the tube is rolled up. The diameter and degree of twist of SWNTs have an essential effect on their electronic properties, leading into metallic conductors or direct band gap semiconductors.

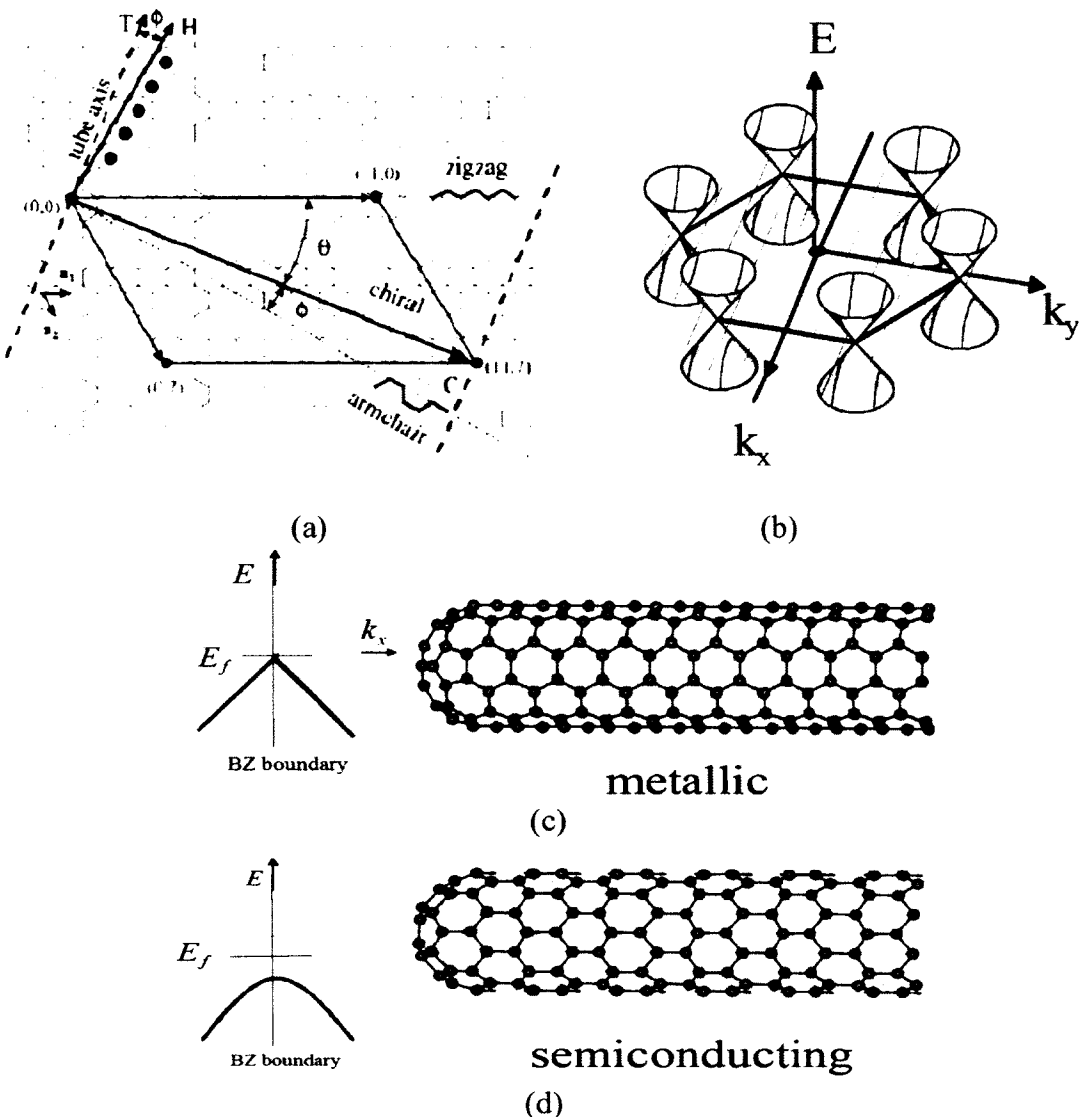


Figure 3. (a) Lattice structure of planar graphene sheet. (Images are from Ref.[3]) (b) Graphene Low Energy Band Structure. (c) Band structure of metallic SWNT. (d) Band structure of semiconducting SWNT. (Images are from Ref.[5])

3.2 Mechanical Property

The nanotube is rolled up by a graphene sheet, which is remarkable strong, thus making the CNT possess exceptional mechanical properties. CNT is a type of material

with high Young's modulus and tensile strength. The Young's modulus of CNT is measured around 1TPa, five times higher than that of steel [47]. CNTs also have extremely high strength, about 63GPa measured, which is much higher than that of the steel (less than 1GPa) [48]. In addition, the CNT is exceptional light, and extremely elastic, capable of bending to a large angle.

3.3 Other Properties

Due to their nano-scale dimension and unusual bonding structure, other properties of CNTs also have been extensively investigated in variety of fields, including chemical, electrochemical, optical, optoelectrical, thermal, etc. CNTs have become a good sensor candidate for gas molecules detector, especial for toxic gas because of its molecular-scale size and extreme sensitivity to environment. Due to the quantum confinement from their cylindrical nature and to their well-defined band and sub-band structure, CNTs possess special optical and optoelectronic properties. In addition, CNTs also show properties with high thermal capacity and thermal conductivity.

4 CNT Gas Sensor

Carbon nanotube provides a promising material for developing gas sensors with high sensitivity, lower cost, small size, and low operation temperature. Variety of gas sensors have been proposed to detect different types of chemical gas molecules such as NH₃, NO₂, CH₄, H₂, CO, SO₂, H₂S, and O₂.

4.1 NH₃ and NO₂ Environmental Sensor

The chemical gas molecules like ammonia and nitrogen dioxide in the air do harm to human-being's health. Ammonia gas is a severe respiratory tract irritant. High concentration of NH₃ not only pose a threat to humans, causing eye irritation and respiratory

tracts of humans, but also detrimentally affect the wildlife, livestock, and growth of agriculture. NO₂ is also a highly toxic gas that can cause respiratory symptoms in humans and adversely influence the agricultural health. Thus, monitoring these kinds of toxic chemical gas molecules in air is of great importance in many fields.

There are many existing chemical sensors with the capability of sensing NO₂ and NH₃, available on the market. Most of these sensors is composed by semiconducting metal oxide materials. In order to gain for high sensitivity, the sensors operate at high temperatures, higher than 500°C.

By contrast, CNT shows a promising sensing material with strong response to some gas molecules even at room temperature. Some studies have shown that physico-chemical adsorption of gas molecules in nanotubes changes the transport properties CNTs due to the charge transfer between the p-type semiconducting CNTs, caused by the electron-donating NH₃ or electron-withdrawing NO₂ gas. Variety of CNT sensors have been proposed and designed based on this phenomenon [49, 50]. However, there are still main drawbacks of CNT chemical sensors, such as the low sensitivity, poor linearity and repeatability, and long recovery time.

4.2 Humidity Sensor

Humidity plays an important role in many fields, such as process control, meteorology, food storage, electrical devices, etc. In order to measure the humidity in high accuracy, extensive studies on humidity sensors have been done over last decades due to their great importance in its wide applications. Currently, some humidity sensors available on the market are designed and fabricated by using ceramic materials. However due to the

property of the sensing material, there are some major drawbacks of ceramic humidity sensors, including low sensitivity and poor reversibility.

Due to their high surface area to volume ratio, CNTs [51, 52] have been extensively investigated to enhance the sensitivity for humidity sensors. Compared with other materials, CNTs also show excellent electronic and mechanical properties, including mechanical flexibility, and high electron mobility. These properties make CNTs a promising material for humidity sensors.

4.3 Other Sensors

Some groups also have investigated the CNTs as a sensing material to detect other gas molecules such as CH₄, H₂, CO, SO₂, H₂S, O₂, etc [53]. There are also some sensor applications in biological and medical areas for sensing and diagnostic purposes [54], especially for portable diagnostic tool with low-power electronics. The CNT-based bio-sensors have demonstrated good environmental sensitivity. Besides, CNTs have been studied extensive in other sensor applications such as temperature sensor, pressure sensor, mass sensor, strain sensor, flow sensor etc. by exploiting it unique excellent properties.

5 Mechanism of CNT Gas Sensing

Theoretical study and experimental data have shown that the sensing principle of CNT sensors varies for different gas molecule detection. Several mechanisms have been proposed to explain the CNT sensor's response to gas molecules as follows.

- 1). It has been demonstrated that the sensitivity of CNT sensor to diverse gases at room temperature is induced through the charge transfer from or to the adsorbed gas due to polar nature of the surface as well as that of the solvent molecule, according to literatures [44, 55]. The density of the main charge carrier is changed by electron-withdrawing

molecules, such as NO_2 , O_2 , or electron-donating molecules, such as NH_3 , resulting in the conductance change of CNT networks.

2). It has been reported that conduction of CNT networks was modulated by the conducting paths formed inside the CNTs or other composites due to the tunneling effect, and the absorption of molecules increases the distance between adjacent nanotubes, resulting in the electrical property change [56, 57].

3). The electrical property is determined dominantly by the Shottky barrier between the CNT networks and metal contacts. Molecular adsorption on the metal contacts induces the conductivity change of CNT sensor by adjusting the barrier height, other than the gas molecules absorption on the inert tube walls [58, 59].

6 Printed Flexible Electronics

Printable flexible electronics has drew extensive attention, due to its ability for mass production in low-cost and large-area flexible electronic circuits, such as inflatable antenna, electronic paper, RF identification (RFID) tag, smart skin, flexible memory [60, 61], and low-cost sensor. However, the performance of the electronics has been limited by semiconducting properties of the printing materials. For instance, organic semiconducting materials, which are widely used in printable flexible electronics, have low carrier mobility (less than $1.5 \text{ cm}^2/\text{Vs}$), resulting in a low operation frequency, thus making this kind of devices only fit for low speed operation, limited to a few kilohertz.

By contrast, carbon nanotube has shown great promises in printable flexible electronics because of its mechanical flexibility and high field effect mobility. In addition, CNT networks can be fabricated using solution-cast or direct-printing method on flexible substrates or conformal surfaces. This would not only enable the development of chemi-

cal sensors on any desired flexible surface, but also allow them to be printed together with other flexible electronic devices, such as flexible thin-film transistors and RF antennas, thereby making it promising for the development of integrated flexible sensors and electronics circuits with integrated sensing, signal processing, and signal transmission and receiving functionalities.

III HUMIDITY EFFECT ON SWNT AND HUMIDITY-DEPENDENT ELECTRICAL MODEL

1 **Background**

Due to their high surface area to volume ratio, nanostructured materials, such as nanowires [62], carbon nanotubes (CNTs) [4, 63, 64], nanoparticles and nanopillars [65, 66] have been extensively investigated to enhance the sensitivity of humidity sensors. Compared with other nanomaterials [62, 65, 66], CNTs also show excellent electronic and mechanical properties, including mechanical flexibility [67], and high electron mobility [68, 69]. These properties make CNTs promising materials for various applications ranging from nanoelectronics [6, 7, 70] to chemical [8] and humidity sensors [71-73].

Compared with a single CNT, CNT networks contain much denser CNTs, and thus can offer much higher sensitivity for sensors. In addition, CNT networks can be fabricated using solution-cast or direct-printing methods on flexible substrates or conformal surfaces [74, 75]. This would not only enable the development of chemical sensors on any desired flexible surfaces, but also allow them to be printed together with other flexible electronic devices, such as flexible thin-film transistors [74-76] and RF antennas, thereby making it promising for the development of integrated flexible sensors and electronics circuits with integrated sensing, signal processing, and signal transmission and receiving functionalities.

Despite the aforementioned advantages, however, knowledge of the SWNT network based humidity sensors is limited. In this paper, we investigate humidity-dependent conductance of SWNT networks. The carrier transport processes is analyzed by performing a temperature-dependent conductance study. Humidity-dependent conductance is modeled and compared with the experimental data. Such knowledge about the humidity effect on the electrical properties of CNT networks will not only benefit reliability studies of the CNT-based flexible electronics, but also facilitate the development of CNT-based humidity sensors with high sensitivity.

2 CNT Network Conductance

However, CNT has rather special features, such as the one-dimensional character of the chains. Many studies have shown that the conduction mechanism in carbon nanotube is similar as the traditional conductor, such as metal-semiconductor transition in disordered materials, such as conducting polymers, polysulphur nitride, etc. [77] It has also been found that the hopping or tunnelling conduction play a critical role in conduction of the CNT networks [78, 79].

2.1 Conductance Based on Carrier Hopping by Thermal Activation

The conductivity of the disordered materials can be explained by variable hopping based on Mott's law. In disordered materials, such as CNT networks, with localized states in the band gap, the conduction can be induced by phonon-assisted tunnelling between electronic localized states, resulting in carrier hopping between inter-junctions of the nanotubes. The adjacent states with accessible energies become less, when the thermal energy $k_B T$ decreases [77]. Therefore, the average hopping range increases. The conductivity of the materials can be written as [80],

$$\sigma(T) = \sigma_{c0} \exp\left\{-\left(\frac{T_0}{T}\right)^\gamma\right\}, \quad (1)$$

where σ is the conductivity of the material, σ_{c0} is a temperature-independent pre-exponential factor, T is the temperature of the material, T_0 is a temperature independent constant, which is given by $k_B T_0$, and γ is a exponential coefficient, determined by the material properties and the temperature. In bulk materials, the exponential coefficient is equal to 1/4.

When the temperature is sufficiently high, the hopping occurs to the closest neighbors. In this situation, the conductivity formula for disordered materials can be expressed in a simple activated form with $\gamma = 1$ in Equation (1). The conductivity, dominantly from the electron transport by thermal excitation, could be approximately proportional to the number of electrons, which are excited across the band gap of the semiconducting material.

2.2 Conductance Based on Tunneling Through the Inter-CNT Barriers

When the electrostatic charging energy is much smaller than $k_B T$ for accessible temperatures, if the metallic regions are sufficiently large, the tunneling in the barrier occurs between metallic states with the same energy without thermal excitation. As the temperature increases, the tunneling current can be increased significantly by the fluctuation in the voltage across the tunnelling junction [81]. For a simple parabolic barrier shape, the conductivity induced by the fluctuation-assisted tunnelling can be derived as,

$$\sigma(T) = \sigma_{r0} \exp\left\{-\left(\frac{T_0}{T + T_l}\right)\right\}, \quad (2)$$

where T_0 is a temperature-independent constant. The parameter T_l indicates the temperature at which the thermal voltage fluctuations become large enough to raise the energy of

electronic states to the top of the barrier. The tunnelling without fluctuations is decided by the ratio T_0/T_I . The pre-factor σ_{T_0} is assumed as a temperature independent constant approximately [77].

3 Experiments

3.1 Device Fabrication

The humidity sensor is a SWNT network based resistor (referred to as “the device” henceforth). Figure 4 (a) shows the microscopic picture of the device. It consists of a pair of Au electrodes and a thin layer SWNT film coated on the Au electrodes. The device was built on a p-type silicon substrate with a 500 nm-thick SiO_2 layer. The thickness of the Au electrodes is 200 nm. The spacing between two Au electrodes, L (i.e., the length of the CNT channel), is 20 μm . The width of the device, W , is 500 μm . Figure 4 (b) shows the atomic force microscopy (AFM) image of the SWNT network film. The SWNT network film was formed by dispensing a drop (approximately 10 μL) of ultrapure SWNT aqueous dispersion (Brewer Science, Inc. (BSI)) onto the Au electrodes on the surface of the silicon substrate. After the solution casting, the device was air-dried and put on a hot plate at 90°C under atmosphere for 30 minutes to improve its stability. A SWNT network film was finally formed across the Au electrodes. The CNT film thickness was estimated to be less than 1 μm [74]. The CNT dispersion is pure water-based, surfactant-free and contains freely suspended SWNTs. The material is purified to remove non-nanotube carbon impurities and catalyst metal particle impurities. The metal content in the water solution is less than 500 ppb. The tubes are functionalized with OH- groups to keep them disperse in the solution.

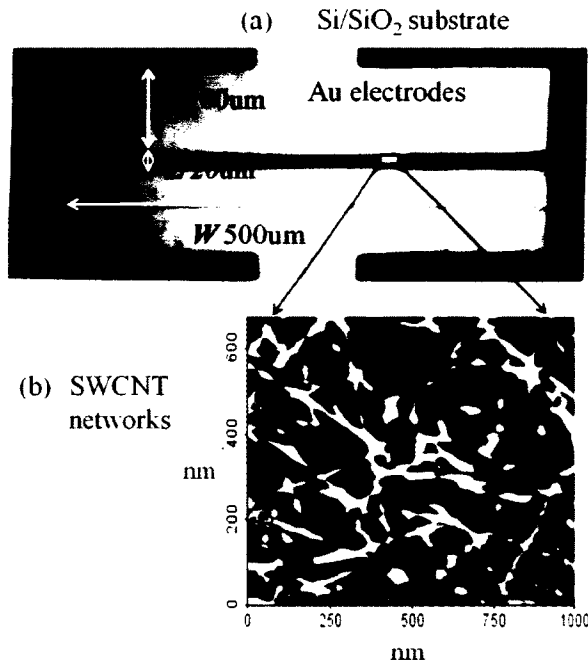


Figure 4. (a) Microscopic picture of the device with two Au electrodes and SWCNT networks on Si/SiO₂ substrate. The length L and the width of the device W are 20 μm and 500 μm , respectively; (b) AFM image of the CNT networks.

3.2 Device Measurement

The device substrate (p-type silicon) is attached to an Au-coated copper plate on the top of a four-stage thermoelectric (TE) module. The TE module was used to control the temperature of the device by a temperature controller (ILX-Lightwave, LDT-5412). The copper plate and the TE module were grounded in the measurement. Since the device is on a p-type silicon substrate that is attached to the grounded copper-plate, the gate of the device is effectively grounded. The electrical characteristics of the device were measured using a Keithley 2602 dual source meter in a controlled humidity chamber, which is a closed chamber with a precise temperature tuning range up to 55 °C and humidity con-

trol resolution of 0.5% relative humidity (RH). The environment temperature is fixed at 304.3K.

4 Results and Discussions

4.1 Contact Resistance

We first determined the contact resistance between the electrode and the SWNT network. The total resistance of the SWNT network based resistor R can be written as [82]:

$$R = 2R_c + R_{sh} \frac{L}{W}, \quad (3)$$

where R_{sh} is the sheet resistance of the CNT networks, R_c is the contact resistance between the CNT network and metal electrode, and L is the spacing between the electrodes. The sheet resistance R_{sh} and the contact resistance R_c can be obtained by the transmission line method (TLM) [83, 84], which need to measures the total resistance R at different channel lengths. Figure 5 (a) depicts the picture of a 4-channel device for R_{sh} and R_c measurement. The channel lengths L are 5, 10, 20, and 40 μm . The width of channel W is 600 μm . Figure 5 (b) plots the measured resistance R at different channel lengths (R-L curve) at the humidity of 4.28 g/m^3 . The R-L curve agrees well with Equation (3). The intercept and the slope of the R-L curve give $2R_c$ and R_{sh}/W , respectively. The R_c and R_{sh} are calculated to be 83.4 Ω and 26.8 $\text{k}\Omega/\text{sq}$, respectively.

Furthermore Equation (3) can also be written in terms of the characteristic length of the SWNT networks L_t as:

$$R = 2R_{sh} \frac{L_t}{W} + R_{sh} \frac{L}{W}, \quad (4)$$

where R_c and L_t are related by:

$$R_c = R_{sh} \frac{L_t}{W}, \quad (5)$$

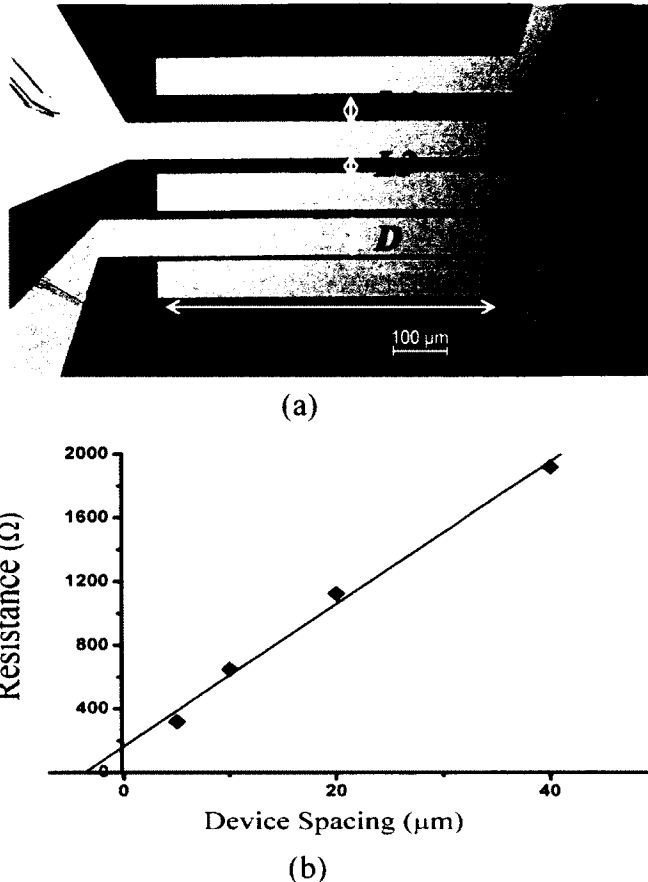


Figure 5. (a) Picture of the 4-channel device for R_{sh} and R_c measurement. The spacings of the channels are 5, 10, 20, and 40 μm. The width of channel is 600 μm and width of the Au electrodes is 60 μm. (b) Device resistance as a function of spacing. The intercept and the slope of the R-L curve give $2Rc$ and R_{sh}/W , respectively.

From Equation (5), the characteristic length of the SWNT networks L_t can thus be obtained to be 1.87 μm. It was also verified that the L_t is quite stable (< 8.7% variation) within the entire humidity range from 4.28 g/m³ to 20.45 g/m³ in our experiment. Since L_t is much smaller than the channel length of the device of 20 μm (see Figure 4 (a)), the

resistance of the device is predominately determined by the resistance of the SWNT networks.

4.2 I-V Characteristics of the Device

Figure 6 shows the I-V characteristics of the device at three different humidity levels, ρ_w , at the device temperature of 312.9K. Linear I-V curves are obtained at the bias voltage range from -2 V to 2 V, indicating ohmic contacts between the CNT networks and the Au electrodes. The slopes of the I-V characteristics give the conductance of the CNT networks. Such linear I-V characteristics allow one to characterize the electrical properties of the CNT networks using the conductance of the SWNT networks. Besides as shown in Figure 6, the conductance of the SWNT networks decreases as the humidity increases.

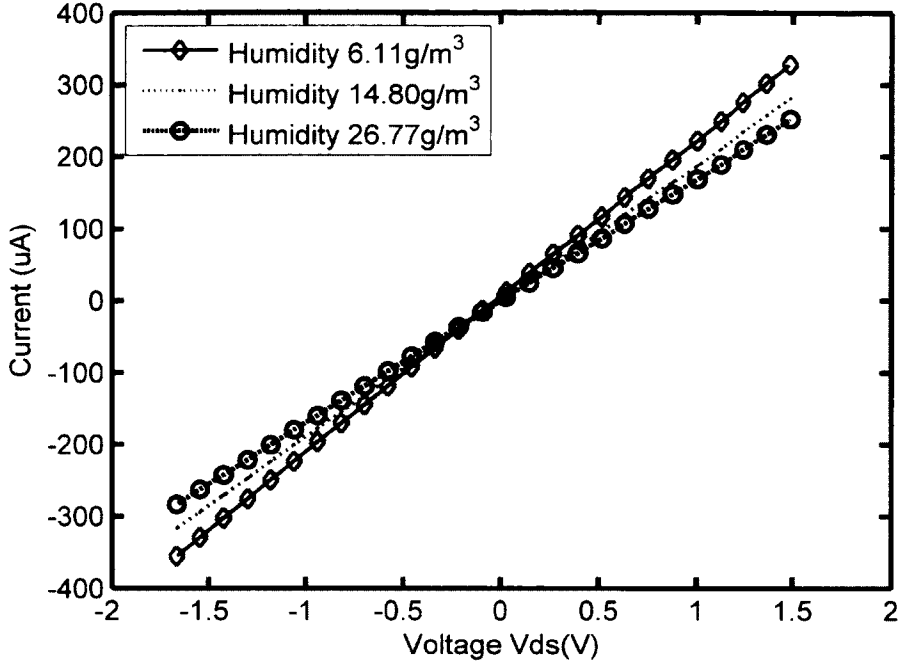


Figure 6. I-V characteristics of the SWCNT networks at three different humidity levels at the device temperature of 312.9K. Linear I-V curves are obtained at the bias voltage range from -2 V to 2 V, indicating ohmic contacts between the CNT networks and the Au electrodes. The slopes of the I-V characteristics give the conductance of the CNT networks.

4.3 Electrical Model

To understand the carrier transport process in the SWNT networks, we investigate the temperature-dependent conductance of the SWNT networks. Figure 7 plots the conductance of the device as a function of the humidity levels for different device temperatures from 312.9 K to 343.1 K. At each temperature, the conductance decreases as the humidity level increases from 6.11 g/m^3 to 28.16 g/m^3 . The conductance increases as the device temperature increases.

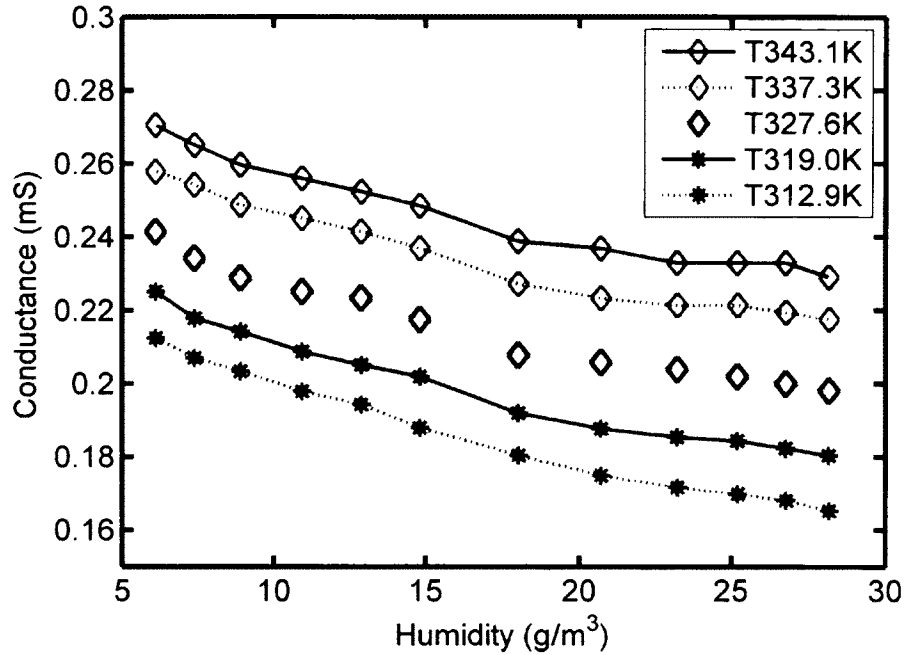


Figure 7. Conductance of the device v.s. humidity levels ρ_w at different device temperature from 312.9K to 343.1K. At each temperature, the conductance decreases as the humidity level increases from 6.11 g/m³ to 28.16 g/m³. The conductance increases as the device temperature increases.

The conductance of the CNT networks G_N depends on two factors: (1) the conductance of CNT itself, and (2) the carrier transportation between the CNTs (inter-CNT carrier transportation). The conductance of CNT itself is determined by the product of the carrier density and the mobility of the carriers. For the carrier transportation between the CNTs, there are two possible parallel carrier transportation mechanisms: (1) carrier hopping by thermal activation, and (2) tunneling through the inter-CNT barriers[77, 81]. The

conductance due to the carrier transportation between the CNT, σ , is proportional

$$\text{to } \exp\left(\frac{-T_1}{T + T_0}\right),$$

$$\sigma = \sigma_0 \exp\left(\frac{-T_1}{T + T_0}\right), \quad (6)$$

where σ_0 is a temperature-independent pre-exponential factor, T_0 is a temperature-independent constant, T_1 is a parameter related to the separation between the CNTs, w . T_1 can be expressed by [81]:

$$T_1 = \frac{SwE_0^2}{8\pi k_B}, \quad (7)$$

where w and S are the separation and the effective contacting area between the CNTs, respectively, and E_0 is the applied electric field that can make the maximum potential barrier $V_m = 0$ (flat band).

In Equation (6), at high temperature, thermally activated carrier hopping will be the dominating carrier transportation process. The conductance due to the thermally activated carrier hopping, σ_{th} , is proportional to $\exp(-T_1/T)$. At $T = 0$ K when there is no thermally activated carrier hopping, the conductance is solely due to the tunneling, i.e.

$$\sigma = \sigma_0 \exp\left(\frac{-T_1}{T_0}\right). \text{ A small } T_0/T_1 \text{ ratio leads to a low conductance.}$$

To obtain the T_0 and T_1 values from experimental data, we take the natural logarithm on both side of Equation (6):

$$\ln \sigma = \ln \sigma_0 + \frac{-T_1}{T + T_0}, \quad (8)$$

Our experimental data show that $\ln \sigma$ v.s $\frac{-T_1}{T}$ plot is quite linear. This indicates that T_0 is small compared to T . The first order approximation of the Equation (6) gives:

$$\ln \sigma = \ln \sigma_0 + \frac{-T_1}{T} + \frac{T_1}{T^2} T_0, \quad (9)$$

In Equation (9), the $\ln \sigma_0 + \frac{-T_1}{T}$ term is the linear approximation of the $\ln \sigma$, whereas the $\frac{T_1}{T^2} T_0$ is the deviation from the linear approximation. Figure 8 shows the $\ln \sigma$ versus $1000/T$ plots for different humidity levels from 6.11 g/m^3 to 26.77 g/m^3 . The circles, diamonds, and stars are the measured data. The solid curves the linear fittings. Very good linearities are obtained for all the humidity levels. The T_1 values can be obtained from the slopes of the linear fittings. The T_1 values of other humidity levels can also be obtained using the same approach. The T_1 values are listed in Table 1.

The deviation from the linear approximation, .. can be obtained by taking the difference of $\ln \sigma$ and its linear approximation. Using the T_1 values in Table 1, one gets the T_0 values, which are also listed in Table 1.

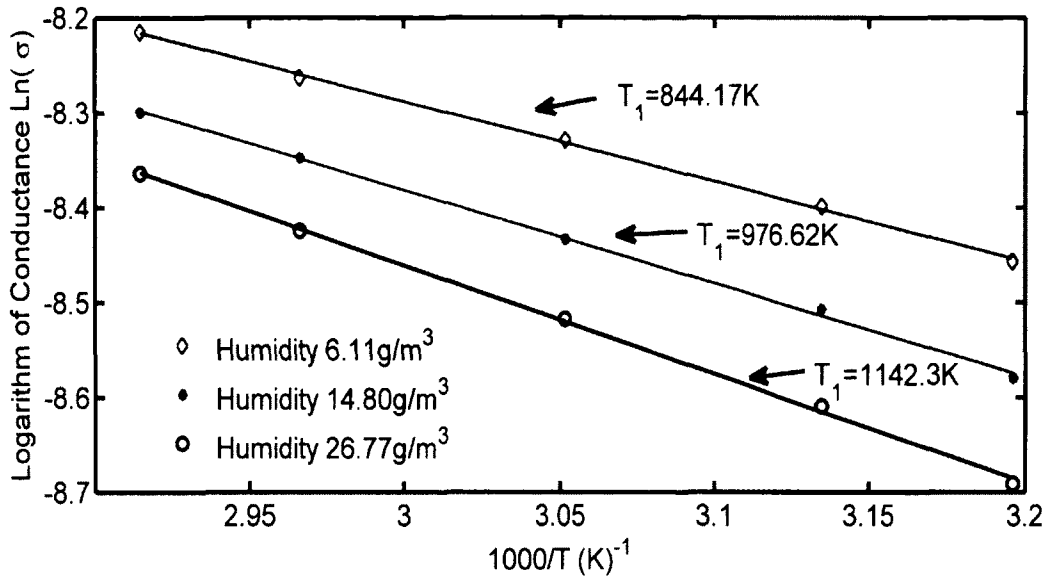


Figure 8. $\ln \sigma$ v.s $\frac{-T_1}{T}$ plot for three different humidity levels ranging from 6.11 g/m^3 to 26.77 g/m^3 . The circles, diamonds, and stars are the measured data. The solid curves the linear fittings. Very good linearities are obtained for all the humidity levels.

Table 1. T_1 and T_0 parameters at different humidity levels obtained by curve fitting.

Humidity(g/m ³)	6.11	8.91	12.87	18.04	20.71	23.17
T_1 (K)	844.17	873.44	938.82	996.74	1064.12	1076.1
T_0 (K)	0.035	0.044	-0.031	0.009	-0.042	-0.105

From Table 1, it is worthy of note that the T_0 values are near zero at all the humidity levels. T_0 can be ignored when compared with the device test temperature of $> 300 \text{ K}$.

Therefore the σ is primarily proportional to $\exp\left(\frac{-T_1}{T}\right)$, i.e.

$$\sigma \approx \sigma_h = \sigma_0 \exp\left(\frac{-T_1}{T}\right), \quad (10)$$

This indicates that the conductance contribution is mainly from the thermally activated carrier hoping and the conductance contribution from the carrier tunneling through the CNT barriers is low.

The conductance of the whole CNT network film can be thus be expressed as:

$$G_N \propto \exp\left(\frac{-T_1}{T}\right). \quad (11)$$

As shown in Equation (7), the T_1 values depend on the separation between the CNTs. We now determine the change of the separation w at different humidity levels. Figure 9 shows T_1 values as a function of the humidity levels, ρ_w . The diamonds are the experimental data, and the solid line is the linear fitting curve. A good linearity between T_1 and the humidity, ρ_w , is obtained with a correlation coefficient of 0.9949. The slope and the interception of the linear fitting are 13.58 K/g/cm^3 and 767.53 K , respectively.

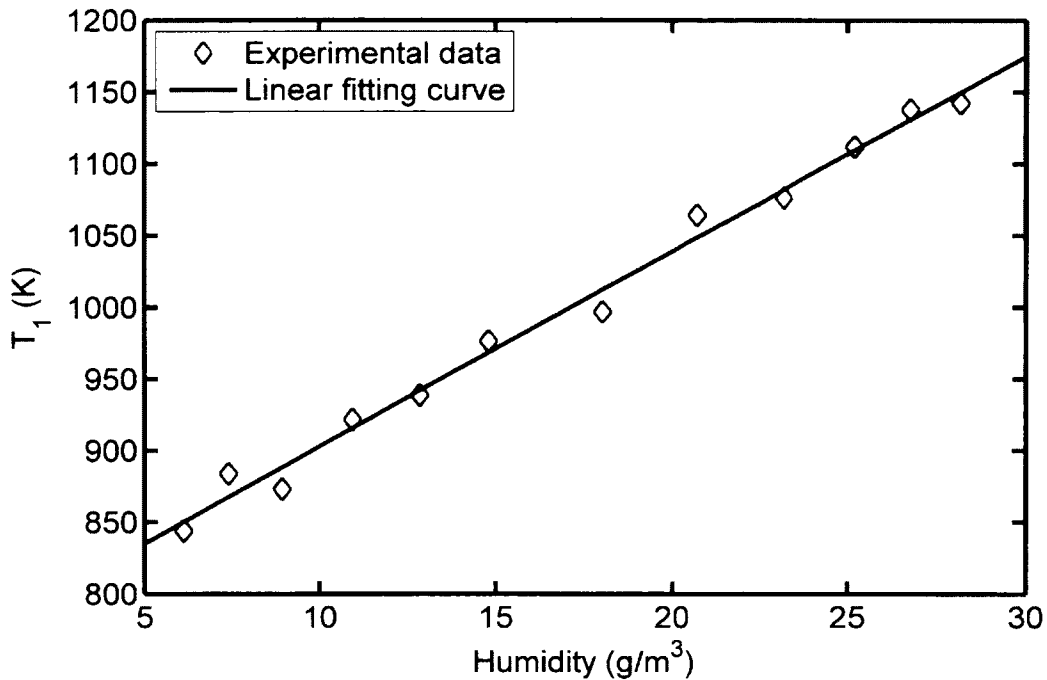


Figure 9. T_l values as a function of the humidity levels, ρ_w . The diamonds are the experimental data, and the solid line is the linear fitting curve. A good linearity between T_l and the humidity, ρ_w , was obtained with a correlation coefficient of 0.9949. The slope and the interception of the linear fitting curves are 13.58 K/g/cm³ and 767.53 K, respectively.

The T_l can thus be written as:

$$T_l(\rho_w) = 13.58\rho_w + 767.53, \quad (12)$$

Equation (12) indicates that the average separation between the SWNTs varies linearly with the humidity levels.

Combining Equation (6) and (12), one obtains the linear relationship of the average separation between the CNTs, w , with the humidity, ρ_w :

$$w = \frac{8\pi k_B}{SE_0^2} (13.58\rho_w + 767.53). \quad (13)$$

The linear relationship of the separation, w , with the humidity, ρ_w , suggests a linear dilution effect, i.e. the CNT separation increases evenly with the humidity levels, ρ_w .

Combining Equation (11) and (12), one gets:

$$G_N = A \exp\left(-\frac{13.58\rho_w + 767.53}{T}\right), \quad (14)$$

where A is a temperature-independent pre-exponential factor. The factor A can be obtained by comparing the experimental data of the CNT networks conductance, G_N , with the calculated values by using Equation (11).

To further investigate the dependence of the factor A on humidity, we plot the factor A in logarithmic scale and at different humidity levels in Figure 10. The stars are the experimental data, and the solid line is the linear curve fitting. A linear relation was obtained between $\ln(A)$ and ρ_w with a linearity of 0.9906. The factor $A(\rho_w)$ can be thus expressed as:

$$A(\rho_w) = \exp(0.0326\rho_w - 5.95), \quad (15)$$

Very similar results were obtained for other temperatures as well, indicating that the factor A is truly temperature-independent. The physics of the humidity dependence of the pre-exponential factor A is not clear and is subject to further research.

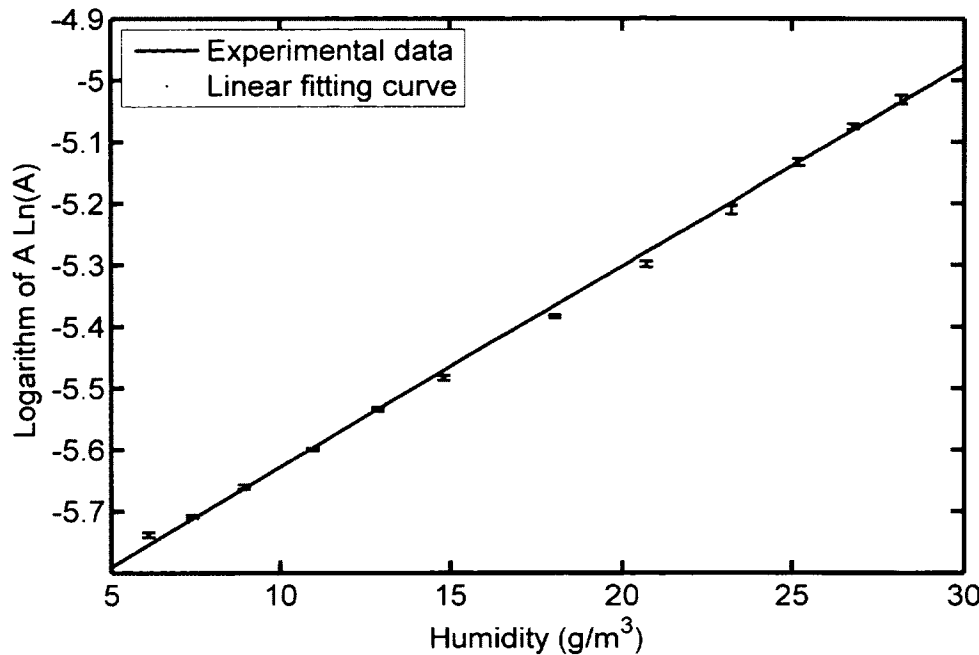


Figure 10. Relationship between the factor A in logarithm scale and different humidity levels at device temperature 312.9K. The stars are the experimental data and the solid line is the linear curve fitting. A linear relation is obtained between $\ln(A)$ and ρ_w with a linearity of 0.9906.

Finally, combining Equation (14) and (15), one can express the model of the SWNT networks conductance at different humidity levels and device temperatures by:

$$G_N(T, \rho_w) = A_0 \exp\left(0.0326\rho_w - \frac{13.58\rho_w + 767.53}{T}\right) \quad (16)$$

where A_0 is a temperature- and humidity-independent constant. $A_0 = 0.0026 S$ for this device.

Figure 11 illustrates the measured conductance of SWNT networks compared with the calculated values using the model in Equation (16) at different device temperatures and humidity levels. The model agrees well with the experimental data.

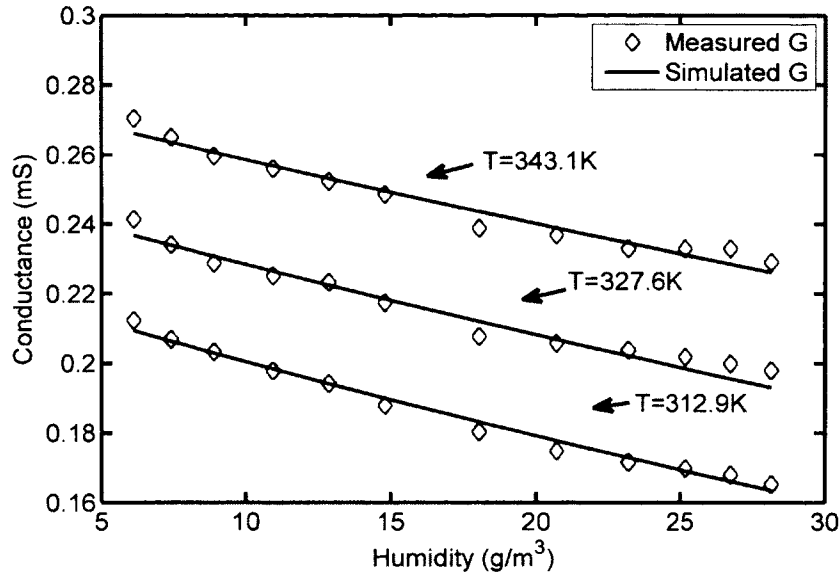


Figure 11. Measured conductance of SWCNT networks compared with the calculated values using the model in Equation (16) at different device temperatures and humidity levels. The model agrees well with the experimental data.

5 Conclusions

In this chapter, we investigated the conductance of the SWNT networks at different humidity levels and device temperatures. It is found that the conductance of the SWNT networks is dominated by the thermal activation carrier hopping over the barriers between the SWNTs. The average separation between the SWNTs increases linearly with the humidity levels. The humidity-dependent conductance of the SWNT network is mod-

eled and compared with the experimental data. The model agrees well with the experimental data.

IV ELECTRICAL MODEL OF SWNT SENSOR FOR AMMONIA AND NITROGEN DIOXIDE SENSING

1 **Background**

Since Iijima's discover [4], Carbon nanotubes have been extensively studied recently. Due to their unique electronic and mechanical properties, CNTs have shown great promises in various applications ranging from nanoelectronics [7] to chemical sensor technology [8]. The adsorption of gas molecules on CNT was reported, and CNT sensors for gas molecules, especially toxic gases, have been proposed by various groups [44, 85]. The high surface to volume ratio of CNT makes the CNTs electrical properties extremely sensitive to the molecules adsorption [86]. Due to its high toxicity, NH₃ and NO₂ is a big concern in many areas, such as industrial, agricultural, medical fields, etc. The threshold limit value for NH₃ exposure for instance, the level of exposure for a typical worker who can experience without an unreasonable risk of disease or injury, is 25 ppm for 8 hours and 35 ppm for only 10 minutes[87]. Thus, monitoring NH₃ and NO₂ in air is of great importance in many fields. Currently, most conventional chemical gas sensors operate at an elevated temperature to get an optimum sensitivity. In contrast, CNT sensor can detect NH₃ or NO₂ in a low concentration at room temperature. Therefore, many groups have designed various chemical sensors using CNTs as an active material, and investigated the variation of the conductance of the CNT networks with the NH₃ adsorption [88, 89].

However, the electrical property model of CNT networks and its dependence on the chemical concentration have not been investigated yet.

In this chapter, the sheet resistance of single-walled CNT (SWNT) networks was measured by transfer length method (TLM) to exclude the effect from contact resistance. The electrical response of SWNT networks of the sensor to NH₃ or NO₂ flow with different concentrations was measured. The concentration dependence of electrical property was investigated, and an electrical sensor model was also developed based on Langmuir adsorption isotherm in this chapter. The experimental data agrees well with the model. The primary objective of the sensor model was to understand the relationship between conductance of CNT networks and NH₃ or NO₂ concentration. With this understanding, the model offers a measurement of chemical molecule concentration based upon the electrical property of CNT sensor. In addition, the mechanism of chemical molecule adsorption on CNT networks was analyzed based on this model. It was found that the sensing mechanism is dominantly determined by the charge transfer in this study. We also compare and analyze different sensing mechanisms for NH₃/NO₂ and H₂O.

2 Sensing Mechanism

To our best understanding, several mechanisms have been proposed to explain the CNT sensor's response to gas molecules as follows.

1). It has been demonstrated that the sensitivity of CNT sensors to diverse gases at room temperature is induced through the charge transfer from or to the adsorbed gas due to polar nature of the surface as well as that of the solvent molecule, according to literatures [44, 55]. The density of the major charge carrier is changed by electron-

withdrawing molecules, such as NO_2 , O_2 , or electron-donating molecules, such as NH_3 , resulting in the conductance change of CNT networks.

2). The electrical property is determined dominantly by the Shottky barrier between CNT networks and metal contacts. Molecular adsorption on the metal contacts induces the conductivity change of CNT sensor by adjusting the barrier height, other than the NH_3 adsorption on inert tube walls [58, 59].

3). It has been reported that the conduction of CNT networks is modulated by the conducting paths formed inside the CNTs or other composites because of tunneling effect, and the adsorption of molecules increases the distance between adjacent CNTs or between CNT and other composites, resulting in the electrical property change [56, 57].

3 Experiments

3.1 Fabrication

Figure 12 (a) shows the device structure of the CNT sensor, consisting of five gold (Au) electrode pads and four active sensing channels with different spacing, $L = 5$, 10, 20, and 40 μm respectively. The device is built on a silicon substrate with a SiO_2 layer with 500 nm thickness. The thickness of the Au electrodes is 200 nm. The width of the device W is 600 μm .

The Si/SiO_2 wafer was cleaned by UV ozone using a corona discharge generator to make it hydrophilic. Then the Si/SiO_2 surface of the substrate was functionalized with aminopropyltriethoxy silane (APTES) by immersed into 1% APTES solution for 10 mins, rinsed with isopropyl alcohol (IPA), and blown dry with nitrogen (N_2) gas. After APTES functionalization, the wafer was immersed into ultrapure aqueous SWNT solution from Brewer Science Inc. for 20 mins. Next, the nanotube solution was blown away from the

wafer surface, and the wafer was blown dry with N₂ [90]. Finally, after the deposition of CNT, the device was thermally annealed on a hot plate at 90°C under atmosphere for 30 mins to improve the stability. The sensor surface of SWNT networks was scanned by Atomic force microscopy (AFM) and the result is shown in Figure 12(b). The electrical property of the SWNT networks as a function of purging time was measured at different ammonia concentrations by using a Keithley 2602 dual source meter in a sensor test chamber at a fixed environment temperature of 19.5°C.

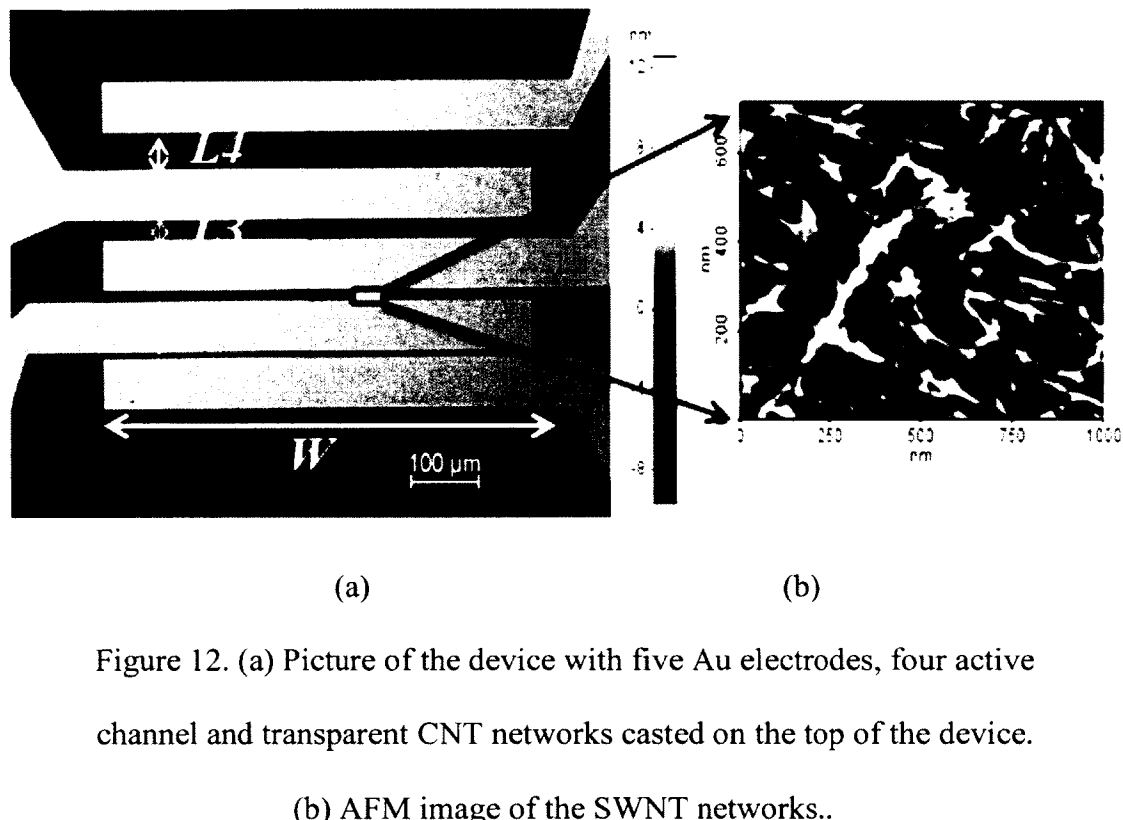


Figure 12. (a) Picture of the device with five Au electrodes, four active channel and transparent CNT networks casted on the top of the device.
 (b) AFM image of the SWNT networks..

3.2 Sheet Resistance Measurement

The sheet resistance is measured at different NH₃ concentration levels by TLM, to exclude the effect from contact resistance between CNT networks and metal contacts. The total resistance of the SWNT networks R can be written as [57, 91]

$$R = R_{sh} \frac{L}{W} + 2R_c \frac{L_t}{W} \quad (17)$$

where the first term represents the CNT network resistance between two adjacent electrodes, R_{sh} is the sheet resistance of the CNT film, L is the spacing between the electrodes (i.e. channel length) and W is the width of the device. The second term at the right hand side of Equation (17) means the contact resistance R_c between the CNT networks and metal electrodes, where L_t is the characteristic length.

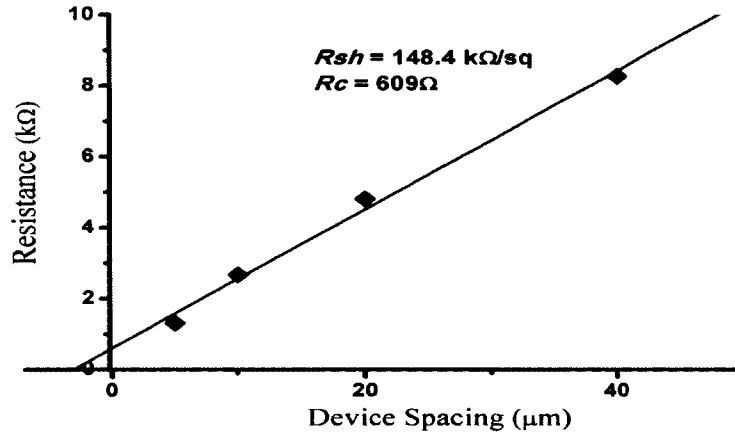


Figure 13. Device resistance as a function of the device spacing. The intercept and the slope of the R - L curve give $2R_c$ and R_{sh}/W , respectively.

Figure 13 shows the plot for R_{sh} and R_c measurement of a 4-channel device. The R - L curve agrees well with Equation (17). The intercept and the slope of the R - L curve

give $2R_c$ and R_{sh}/W , respectively. With a fitting method, the Rc and Rsh of one device used in the experiment are calculated to be $609.1\ \Omega$ and $148.4\ k\Omega/\text{sq}$ respectively when the initial total resistance keeps stable, purged by nitrogen gas during the experiment.

3.3 Conductance Model for SWNT Networks

The adsorption of gas molecules on SWNT is assumed as a chemical doping process [43]. The carrier concentration n_{CNT} in a doped carbon nanotube can be obtained by adding an impurity concentration induced by the carrier transfer of NH_3 molecules, and is given by [92]

$$n_{CNT} = n_{p0} + n_{gas} \quad (18)$$

where n_{p0} is the initial carrier concentration in carbon nanotubes without NO_2 or NH_3 adsorption, and n_{gas} is the impurity concentration in carbon nanotubes. It was found that the adsorption of gas molecules induces donation or withdrawal of electrons [43]. Assuming that the impurity concentration n_{gas} is proportional to the amount of gas molecules adsorbed on CNT networks, we obtain $n_{NH_3} = kn_{ad}$, where n_{ad} is the concentration of the chemical gas molecules, which is adsorbed onto the surface of SWNTs, and k is the constant coefficient, indicating the average number of electrons donated per adsorbed chemical molecule into the SWNT valence band.

From Drude conductivity relation $\sigma = q\mu_p n_{CNT}$, where σ is the conductivity, q is the electronic charge, and μ_p is the hole mobility, we can see that, if the mobility keeps constant, the conductivity of the nanotube increases with the carrier density linearly [93].

Plugging the carrier concentration Equation (18) into Drude conductivity relation, and further being multiplied by the thickness of CNT film t , we obtain the sheet conductance of the CNT networks as below,

$$\sigma_{sh} = \sigma_{sh0} + q\mu_p t(kn_{ad}) \quad (19)$$

where the first term $\sigma_{sh0} = q\mu_p n_{p0}t$ is the initial sheet conductance of CNT networks without NH₃ or NO₂ doping, and the second term indicates the sheet conductance change induced by the gas molecules adsorption.

3.4 Langmuir isotherm

The adsorption of gaseous molecules on SWNTs has been modeled by the Langmuir isotherm model. The adsorption rate is approximated as follows,

$$r_{ad} = \frac{n_{ad}}{N_{sat}} = \frac{K_L \rho_{gas}}{(1 + K_L \rho_{gas})} \quad (20)$$

where and N_{sat} is the saturation concentration of gas molecules adsorbed on CNT networks (#/cm³), K_L and n are Langmuir constants related to the adsorption capacity and the adsorption intensity of the chemical gas molecules, and ρ_{gas} is the gas molecules concentration (ppm).

Plugging the Langmuir isotherm model into Equation (19), we obtain the sheet conductance of the CNT networks as below,

$$\sigma_{sh} = \sigma_{sh0} + \frac{q\mu_p t k N_{sat} K_L \rho_{NH_3}}{1 + K_L \rho_{NH_3}} \quad (21)$$

The sheet conductance change, induced by gas molecules adsorption, can be further expressed by $\Delta\sigma_{sh} = \frac{\alpha K_L \rho_{gas}}{1 + K_L \rho_{gas}}$ from Equation (21), where the sheet conductance change $\Delta\sigma_{sh} = \sigma_{sh0} - \sigma_{sh}$ and the coefficient $\alpha = q\mu_p t k N_{sat}$. Taking reciprocal both sides of equation, we will obtain as below,

$$\frac{1}{\Delta\sigma_{sh}} = \frac{1}{\alpha K_L} \left(\frac{1}{\rho_{gas}} \right) + \frac{1}{\alpha} \quad (22)$$

By linear fitting between $\frac{1}{\Delta\sigma_{sh}}$ and $\frac{1}{\rho_{gas}}$, one can obtain the values for the coefficients of K_L and α .

4 Results and Discussions

4.1 Electrical Property Model Based Langmuir Isotherm

The response of the SWNT sensor to different chemical gas concentrations was characterized by the gas test system. First, the sensors were purged with nitrogen (N_2) gas for 100 to 380 minutes to make the sensor with a stable initial resistance without chemical gas adsorption. Then, the sensor was exposed to ammonia at a certain concentration level. The conductance value of CNT networks becomes stable enough (i.e. the change rate $< 0.9 \Omega/\text{min}$), then the ammonia gas was switched to a higher concentration level for another 50 mins. The resistance of the sensors was measured at room temperature 19.5°C .

Figure 14 shows the time response of sheet resistance of SWNT networks, when exposed to NH_3 gas with increasing concentrations from 0 to 40.70 ppm. The resistance of the SWNT sensor dramatically increases after being exposed to NH_3 at room tempera-

ture. Especially, when the NH_3 concentration is low, the sensor is much more sensitive. When the concentration goes higher, the sensor is becoming saturated gradually.

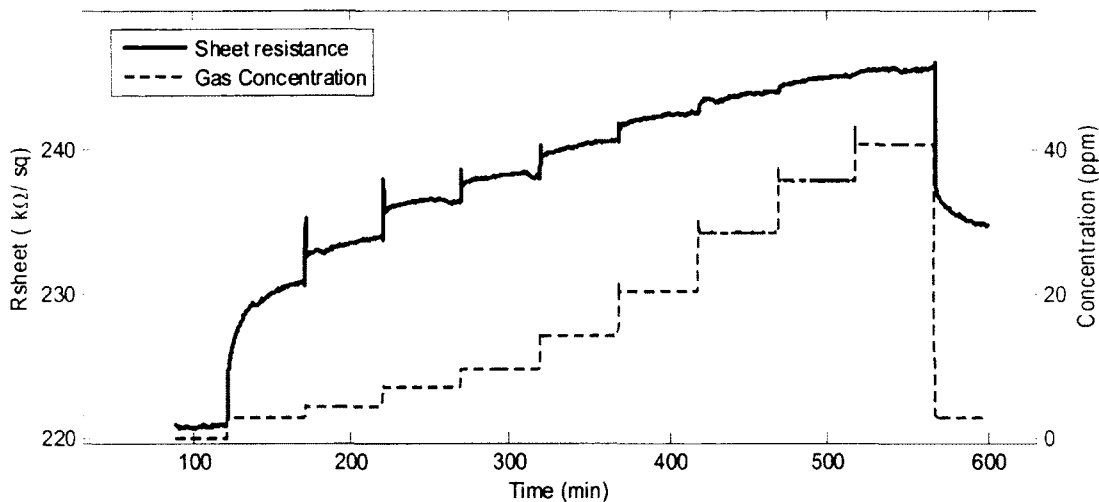


Figure 14. Time response of electrical property of SWNT networks to different NH_3 concentrations from 0 to 40.70 ppm at room temperature.

Figure 15 (a) illustrates the calibration curve of the CNT sensor response to increasing NH_3 concentrations at room temperature with an initial sheet resistance of 228.72 $\text{k}\Omega/\text{sq}$. The plot shows $\frac{1}{\Delta\sigma_{sh}}$ (the sheet conductance change) as a function of $\frac{1}{\rho_{gas}}$ (the reciprocal of NH_3 concentration). In this figure, the diamonds denote the experimental data and the solid line is the linear fitting curve by using Equation (22). A fitting curve is obtained with a correlation coefficient of 0.9971, demonstrating a good match of the Langmuir isotherm model to NH_3 adsorption on CNTs. The coefficients, $\frac{1}{\alpha K_L}$ and $\frac{1}{\alpha}$, are determined by the slope and the interception of the linear fitting curve, respectively.

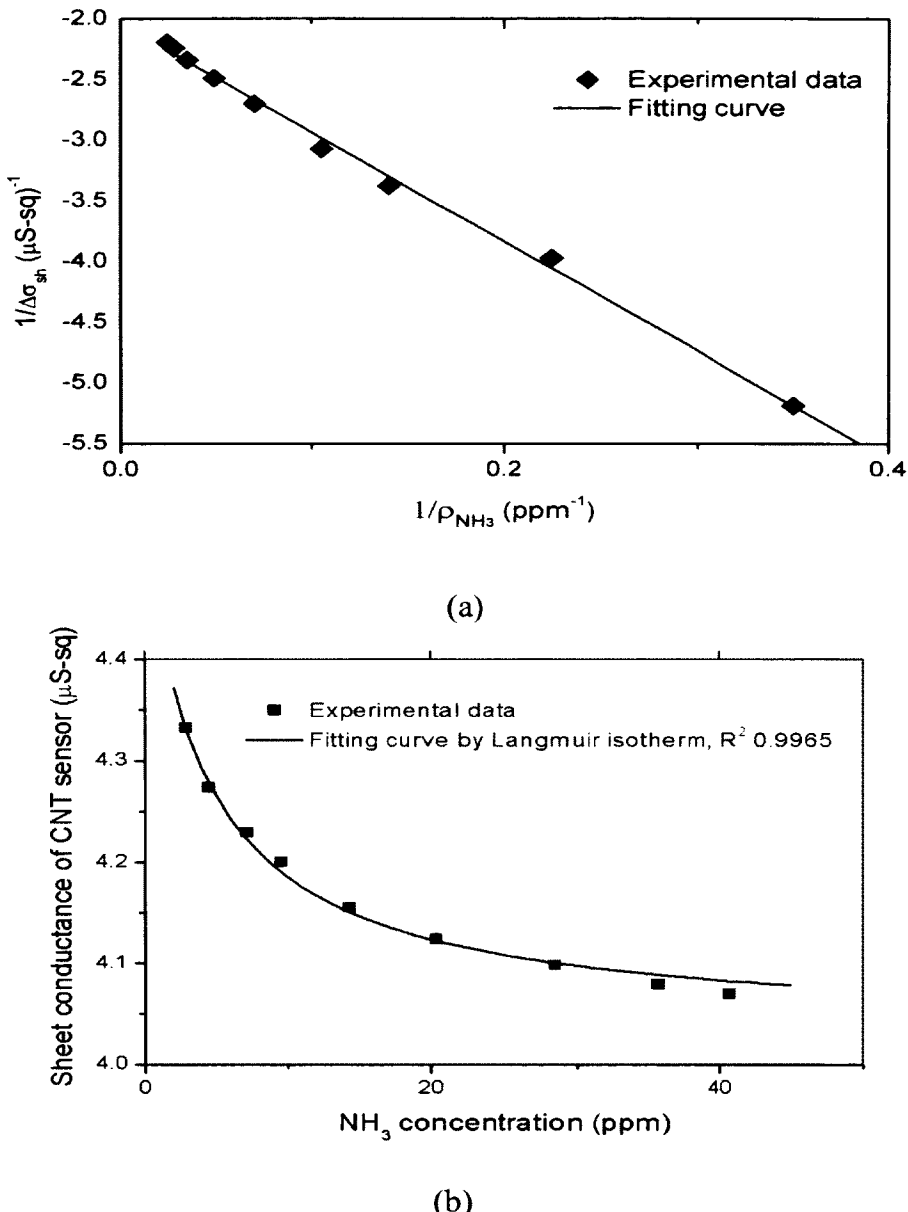


Figure 15. NH₃ sensing experiment. (a) $1/\Delta\sigma_{sh}$ (reciprocal of the sheet conductance change) as a function of $1/\rho_{\text{gas}}$ (reciprocal of NH₃ concentration). (b) Measured sheet conductance of SWNT networks, compared with the calculated values by using the model in Equation (22).

Figure 15 (b) shows the measured sheet conductance of the SWNT sensor compared with the calculated values at different NH_3 concentrations by using the model in Equation (22) with the coefficients calculated by the fitting method as shown in Figure 15 (a). The experimental data agrees well with the model.

We also carried out experiment for NO_2 sensing with the SWNT sensor, following similar steps described at the beginning of this section, but with longer exposure time for each concentration level, in order to get a stable read-out of the sheet resistance.

Figure 16 shows the time response of sheet resistance of SWNT networks, when the CNT networks are exposed to NO_2 gas with increasing concentrations from 0 to 8.57 ppm. The response of the SWNT sensor to different NO_2 concentrations was characterized by the gas test system. From Figure 16, we found that the resistance of the SWNT sensor dramatically decreases after being exposed to NO_2 at room temperature.

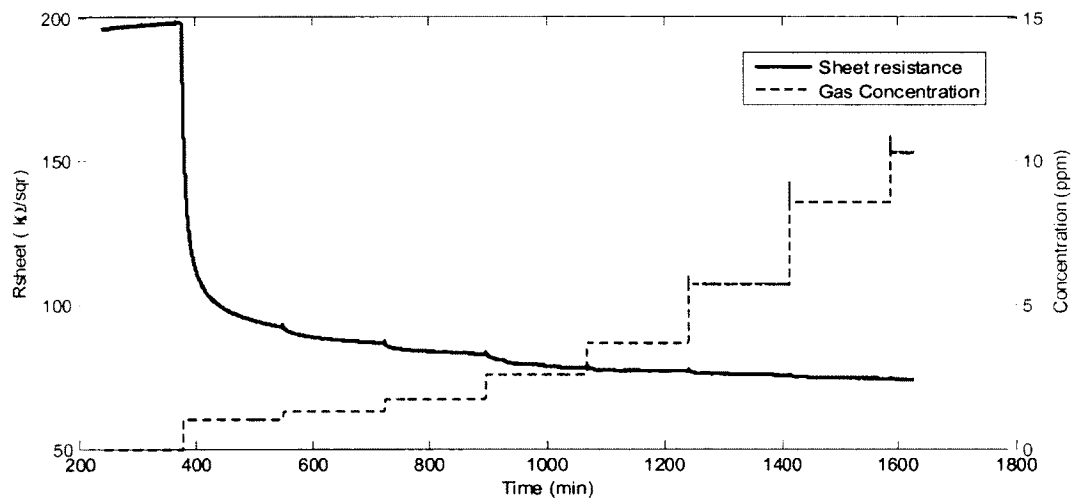


Figure 16. Time response of SWCNT sensor to different NO_2 concentrations from 0 to 8.57 ppm at room temperature.

Figure 17 (a) illustrates the calibration curve of the CNT sensor response to increasing NO_2 concentrations at room temperature with an initial sheet resistance of 198.23 k Ω/sq . The plot shows $1/\Delta\sigma_{sh}$ (the reciprocal of the sheet conductance change) as a function of $1/\rho_{gas}$ (the reciprocal of NO_2 concentration). In this plot, the squares denote the experimental data and the solid line is the linear fitting curve by using Equation (22). A fitting curve is obtained with a correlation coefficient of 0.987, demonstrating a good match of the Langumir isotherm model to NO_2 adsorption on CNTs. The coefficients, $\frac{1}{\alpha K_L}$ and $\frac{1}{\alpha}$, are determined by the slope and the interception of the linear fitting curve, respectively.

Figure 17 (b) shows the measured sheet conductance of the SWNT sensor compared with the calculated values at different NO_2 concentrations by using the model in Equation (22) with the coefficients calculated by the fitting method as shown in Figure 17 (a). The experimental data agrees well with the model.

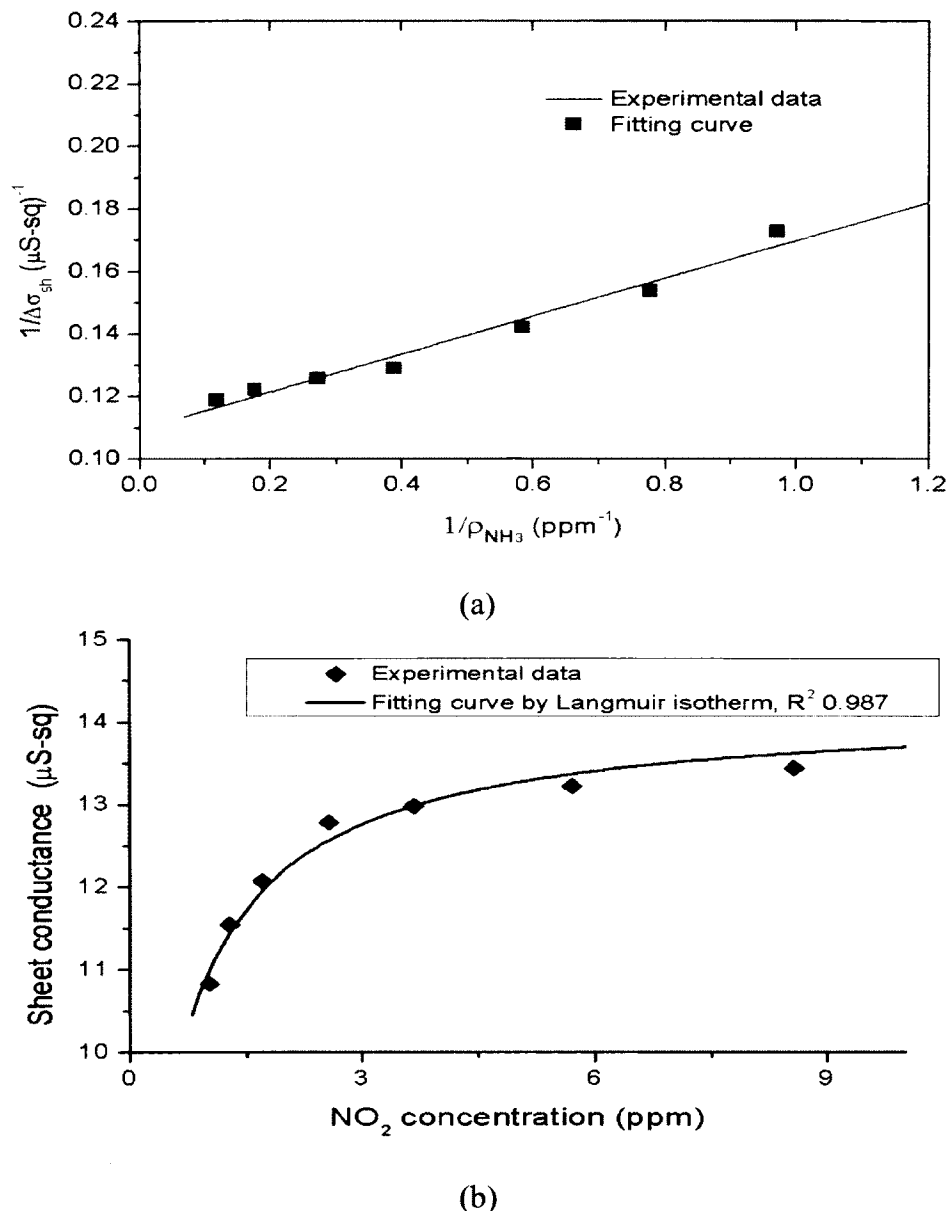


Figure 17. NO_2 sensing experiment. (a) $1/\Delta\sigma_{sh}$ (reciprocal of the sheet conductance change) as a function of $1/\rho_{\text{gas}}$ (reciprocal of NO_2 concentration). (b) Measured sheet conductance of SWNT networks, compared with the calculated values by using the model in Equation (22).

4.2 Sensing Mechanism Analysis

As discussed previously, there are mainly three mechanisms, which have been proposed to explain the CNT sensor's response to gas molecules.

To investigate which mechanism dominates in this experiment, the current and the voltage curve of the CNT senor is measured in this study. First, the linear relationship between the current and the voltage indicates the ohmic contact between the metal pads and SWNT networks [57] This result excludes the sensing mechanism (2), which is determined by the Shottky barrier between CNTs and metal contacts.

Moreover, if the mechanism (3) (tunnel effect between CNT interjections) plays a major role, the resistance of the sensor always increases as increment of the separation between SWNTs, resulting in low tunneling probability, which is caused by increasing gas molecules concentration. But Figure 17 shows that the resistance of SWNT networks decreases as the NO₂ concentration goes higher. It suggests that some different mechanism other than mechanism (3) dominates in this experiment.

Last, Figure 15 and Figure 17 show a good match between the experimental data and simulated data by chemical concentration-dependent conductance model based on Langmuir adsorption isotherm with high correlation coefficients. The NH₃ molecules adsorption on CNT networks introduces charge transfer (electrons donation) from NH₃ molecules to CNTs, resulting in the Fermi level shift far from valence band of CNTs. While, NO₂ molecules adsorbed on CNT networks withdraw electrons from CNTs to NO₂ molecules, resulting in the Fermi level shift far towards the valence band of CNTs. It indicates that the sensing mechanism in this study is dominantly determined by charge transfer through NH₃ adsorption.

4.3 Comparison of Sensing Mechanism for NH₃/NO₂ and H₂O

The experimental results show that the thermal activation carrier hopping over the barriers between CNTs plays a dominate role in humidity sensing, while charge transfer induced by gas molecules adsorption is the main mechanism in NH₃ and NO₂ sensing. It could be explained as following:

First, the binding energy between different gas molecules to SWNT surface is different depending on the gas property. Theoretical study has shown that the binding energy of NH₃ and NO₂ is higher than that of H₂O. Using density functional theory, it indicates that electron charge transfer is the dominate mechanism of the conductivity change in carbon nanotubes upon exposure to NH₃ and NO₂ via physisorption. Moreover, the binding energies between CNT and NH₃, CNT and NO₂ are predicted to be -0.18 eV and 0.42 eV respectively [43]. By contrast, the binding energy between H₂O and CNT is estimated to be 0.035 eV for the 5×5 tube and 0.04 eV for 3×3 tube for the lowest-energy structure [72], suggesting the interaction between water molecules and CNTs is weaker than that of NH₃ or NO₂.

Secondly, dewing effect of humidity on SWNTs plays an important role in CNT humidity sensor, especially when the humidity increases to a very high level. The water vapor in a volume of humid air will condense into liquid water at the surface of the CNTs, particularly in the junctions between CNTs. The liquid water increases the gap distance, resulting in higher barriers between CNTs. Thus, the carrier hopping over the barriers between CNTs dominates in humidity sensing. While, in NH₃ and NO₂ sensing, the gas concentration is extremely low (in ppm level), therefore there is almost no dewing effect, compared with the water concentration.

5 Conclusions

The electrical property model of a SWNT chemical gas sensor with dependency upon gas concentration has been studied. The sheet resistance of SWNT networks was measured by TLM to exclude the effect from contact resistance. The electrical response of SWNT networks of the sensor to NH₃ and NO₂ flow with different concentrations was characterized. The chemical gaseous molecule concentration dependence of electrical property was investigated, and a conductance model of the CNT sensor was also developed based on Langmuir adsorption isotherm. The model agrees well with the experimental data with high correlation coefficient.

It was found that the sensing mechanism is dominantly determined by charge transfer in this study. We also compare and analyze different sensing mechanisms for NH₃/NO₂ and H₂O.

V FLEXIBLE SWNT GAS SENSOR

1 **Background**

Over the last decade, flexible sensor has attracted much attention due to its capability of providing a cost-efficient solution to large-area, thin, lower and conformal profiled applications, such as biomedical sensors for healthcare examinations, gas environmental sensors, smart skins, etc [94, 95]. Since its discovery, carbon nanotube has shown great promises in printable flexible electronics[96, 97], particularly in flexible chemical gas sensors [98], because of its unique properties, such as mechanical flexibility, high surface to volume ratio, semiconductivity, etc. Due to limitations of the fabrication approach, only few flexible CNT sensors have been proposed for sensing toxic chemical gas of ammonia (NH_3) and nitrogen dioxide (NO_2). Yang, et al. designed a wireless flexible SWNT gas sensors to detect NH_3 at extreme high concentration of 4% consistency [99]. A simple all-CNT electronic nose has been proposed to detect NO_2 down to 2.3 ppm [100]. But in their reports the sensitivity and flexibility are not characterized over a certain range of concentrations. A flexible CNT sensors for NO_2 detection have been demonstrated by a flexible, all-organic chemiresistor, with a sensor resistance response <90% to NO_2 at 100 ppm (sensitivity <0.9%/ppm) [98]. However, due to limitations of sensing materials and fabrication approach, these flexible sensors suffer main obstacles for practical usage, such as low sensitivity, high limit of detection, etc. A practical flexi-

ble gas sensor has to be sensitive, and also be able to detect analytes at low concentrations, which should be below the threshold limit value, defined as the level of exposure for a typical worker who can experience without an unreasonable risk of disease or injury. This level is 25 ppm for 8 hours to NH₃ exposure, and 5 ppm to NO₂. Therefore, to design a flexible CNT gas sensor with high sensitivity, low detectable concentration, and flexibility still remains a challenge.

In this chapter, we report a flexible SWNT gas sensor with printed interdigitated electrode (IDE). The response of the flexible sensor was characterized by being exposed to gaseous chemical gas (NH₃ and NO₂) with successively increasing concentrations. The linearity and flexibility of the sensor were analyzed. The flexible SWNT senor exhibits a low limit of detection (LOD) and high sensitivity, 1.32%/ppm for NH₃ detection, and 6.17%/ppm for NO₂, which is much higher than that of other flexible CNT sensors [98-100].

2 Sensor Fabrication

Figure 18 (a) shows the picture of the flexible SWNT sensor, consisting of an IDE printed by using nano silver ink (Figure 18 (b)) and a transparent layer of SWNT thin film coated on the top of the electrodes. The IDE finger width is 380 um, the gap between each finger is 180um, and the length of the IDE is 1400 um.

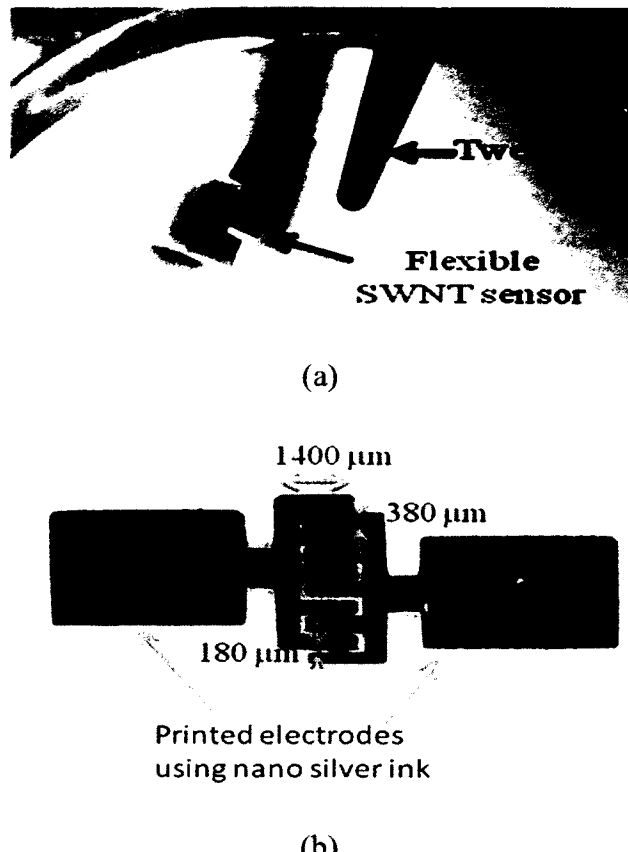


Figure 18. Flexible SWNT sensor with IDE and transparent SWNT film (a) Picture of flexible SWNT sensor. (b) Interdigitated electrodes printed by using nano silver ink

The sensor was fabricated by two major steps, including electrodes printing and SWNT film deposition. First, UTD Ag silver nanoink from UT-Dots was used to print the IDEs on a transparent flexible Kapton polyimide film using an Aerosol Jet® printing system from Optomec, Inc. The substrate and printed IDEs were then heated at 130 °C for 30 mins for thermal annealing. Secondly, the SWNT film layer was deposited by drop-casting ultrapure SWNT dispersion (Brewer Science, Inc.) onto the flexible substrate with the printed IDEs. The ultrapure SWNT dispersion is water-based and surfactant-free containing less than 500 parts per billion (ppb) metal impurities in the dispersion. The

SWNTs were functionalized with OH- groups to keep them dispersed and freely suspended in the solution[57]. Finally, the sensor device was placed on a hot plate at 90°C under atmosphere for 30 min to improve the stability.

3 Experiment

The electrical property of the sensor as a function of purging time was measured by a dual source meter (2602, Keithley) in a sensor test chamber at room temperature. The chemical gas concentration in the test chamber is regulated by a gas generator (OVG4, Owlstone, UK) loaded with a NH₃ or NO₂ permeation tube (VICI Metronics). The time response of the electrical property of the sensor is characterized by being exposed to the gaseous toxic chemical gas with successively increasing concentrations controlled by the gas generator. The sensor is initially purged with N₂ gas for 120 mins to make the sensor resistance stable. Then, the sensor is exposed to the gas flow with a certain NH₃ concentration for 20 mins and purged by N₂ gas for 20 mins, alternatively. The max steady-state resistance is extracted as the response of the flexible CNT sensor at each gas concentration.

4 Results and Discussions

4.1 Electrical Property Characterization

Figure 19 shows the I-V characteristic curve of the flexible SWNT sensor, measured with pure nitrogen (N₂) gas purging at room temperature. Linear I-V curve was obtained at the bias voltage range from -1 V to 1 V, indicating ohmic contact between the SWNT networks and the printed silver IDE. Thus, the conductance of the SWNT networks can be determined by the slope of the I-V curve. Moreover, the linear I-V charac-

teristics allow one to characterize the electrical properties of the sensor by the conductance of the SWNT networks.

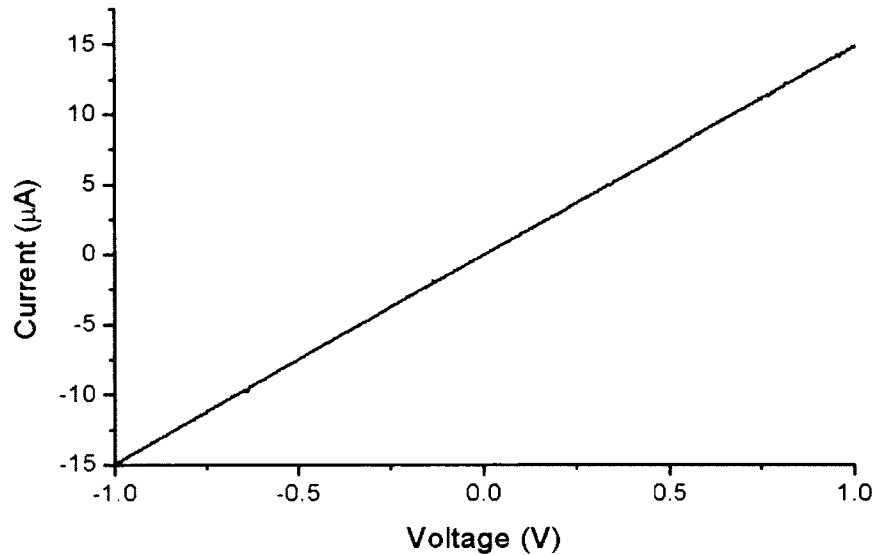


Figure 19. I - V curve of the flexible CNT sensor, measured with N_2 gas purging at the room temperature. A good linear relation is obtained, indicating ohmic contacts between SWNT networks and silver electrodes. The slope of the curve gives the value of the conductance of the flexible CNT sensor.

4.2 Response to Gas Exposure

The sensor is initially purged with N_2 gas for 120 mins to stabilize the resistance of the sensor. Then, the sensor is exposed to the NH_3 flow with different concentrations for 20 mins until the resistance is stabilized. The sensor is purged by N_2 gas for 20 mins before each measurement. The resistance is extracted at each NH_3 concentration. The NO_2 gas sensing follows the same measurement procedures.

We found that the resistance of the sensor increases with the concentration of the NH₃ gas (as shown in Figure 20), whereas it decreases with the concentration of the NO₂ gas (as shown in Figure 21Figure 20).

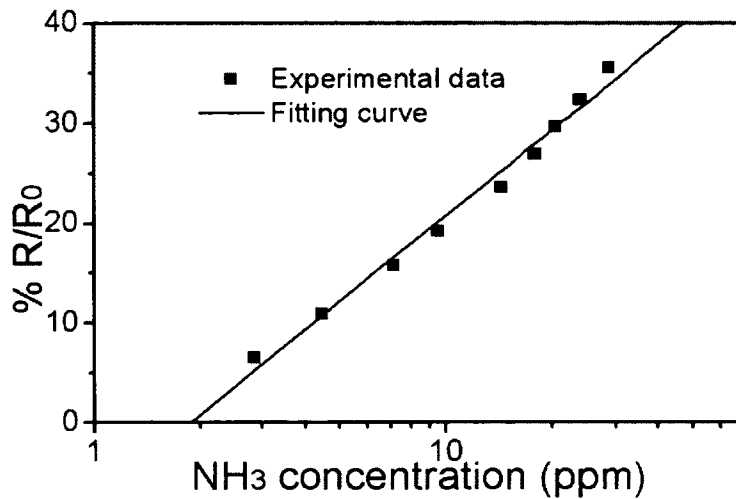


Figure 20. The response of the flexible SWNT sensor to NH₃ gas flow with different concentrations. The squares are the measured data, and the line is linear fitting curve between $\Delta R/R_0$ and the chemical gas concentration in logarithmic scale.

The percentage relative resistance change of the flexible SWNT sensor can be determined by

$$\Delta R/R_0 = (R - R_0)/R_0 * 100\% \quad (23)$$

where R_0 is the initial resistance value of the sensor before it is exposed to the chemical gases, and R is the steady-state resistance value at each gas concentration.

Figure 20 shows the response curve of the relative resistance change $\Delta R/R_0$ as a function of NH₃ concentrations. A good linear relation with a correlation coefficient (R^2) of 0.9932 is obtained between the relative resistance change and the NH₃ concentration in

logarithmic scale in the concentration range investigated in the experiment. A good linearity suggests a sensing signal with high signal-to-noise ratio (SNR) of the flexible sensor. The sensor can detect a minimum NH_3 level of 2.85 ppm at room temperature without any external aids such as a vapor concentrator, or a sensor heater. The minimum detection level is much lower than the CNT gas sensor reported previously [99].

Moreover, the flexible sensor has a significant relative resistance change of 6.52% when exposed to the NH_3 at the lowest concentration of 2.85 ppm. It indicates an even lower LOD could be obtained if the concentration goes lower by the test system.

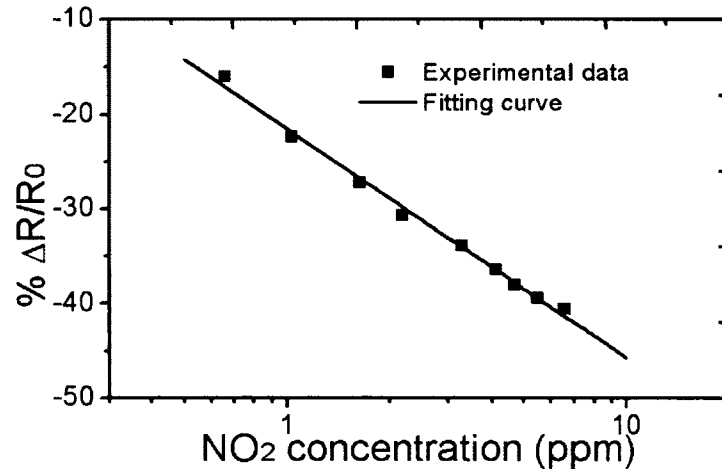


Figure 21. The response of the flexible SWNT sensor to NO_2 gas flow with different concentrations. The squares are the measured data, and the line is linear fitting curve between $\Delta R/R_0$ and the chemical gas concentration in logarithmic scale.

Figure 21 shows the resistance response of the flexible sensor when exposed to NO_2 from 659 ppb to 6.57 ppm. The experimental data also shows a high linearity of 0.9971 between $\Delta R/R_0$ and the NO_2 concentrations in logarithmic scale. Moreover, one can see that the flexible sensor has an extremely high relative resistance change of -

16.0% when exposed to NO₂ at the lowest concentration of 659 ppb in this report. Therefore, a significantly low LOD can be obtained by this flexible SWNT sensor.

Also, the experimental data shows the sensor resistance drops upon NO₂ exposure, by contrast the resistance increases upon NH₃ exposure. This could be caused by the transfer of carrier charge between the CNTs and gas molecules due to the polar nature of the surface as well as that of the solvent molecule [44]. The major charge carrier density is changed by the adsorption of electron-withdrawing molecules, such as NO₂, O₂, or electron-donating molecules, such as NH₃, resulting in the conductance change of SWNT networks.

4.3 Sensitivity Analysis

We define the sensor sensitivity as the relative resistance change per ppm as follows,

$$S = (\Delta R/R_0)/\Delta \rho, \quad (24)$$

where $\Delta \rho$ is the concentration range of chemical gas molecules in the measurement.

A high sensitivity of 1.32%/ppm is obtained for NH₃, and 6.17%/ppm for NO₂, much higher than that of other flexible CNT sensors [98-100]. The high sensitivity could result from the high pure semiconducting SWNT film used as the sensing layer in this report. Semiconducting SWNTs show higher sensitivity than the metallic CNTs [44]. The same SWNT has been used in other CNT electronics with high performance in our previous research [57, 97, 101].

4.4 Flexibility Test

Figure 22 shows the plots of resistance change rate as a function of the bending angle (θ) from -90° to 120° for the flexibility test. The variation of electrical property up-

on the bending could be induced by the band-gap change of the semiconducting SWNT itself [102], or the tunnelling effect between CNTs [103, 104]. When the flexible sensor is bent at a positive angle, the SWNT networks attached on the flexible substrate expands, causing the junction spacing between CNTs or the energy gap increased, resulting in the resistance increase. On the other hand, when the flexible sensor is bent at a negative angle, the SWNT networks are compressed, causing the junction spacing between CNTs or the energy gap reduced, resulting in a decrease of the resistance. The experimental data shows that the total sensor resistance is changed by <6.3%, even when the sensor is bent up to 120°, suggesting good flexibility of the sensor. In addition, the sensor remains a stable resistance when the bending angle is beyond ±20°. Good electrical performance of the CNT sensor under an applied stress may result from the stable and dense CNT networks deposited on the flexible substrate.

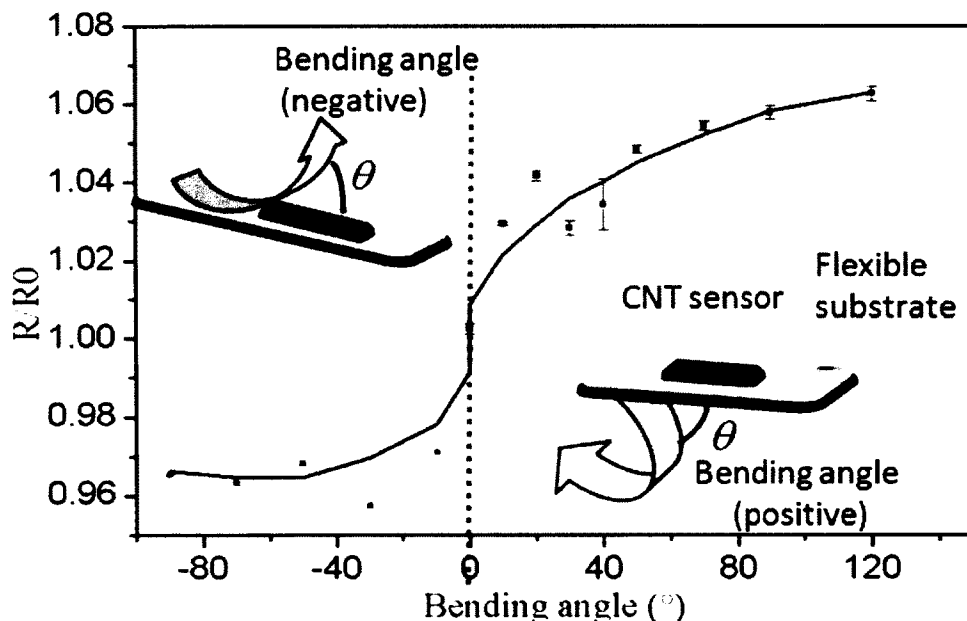


Figure 22. Resistance change rate dependent on the bending angle of the flexible sensor.

However, it was found the conductance of the sensor decreased substantially, after the sensor was creased to 180° more than ten times. It may be caused by the deformation or cracks of the CNT film or the silver electrodes. Then, the sensor response was characterized with a bending angle fixed at 90°. Though the initial conductance decreases, the sensor still exhibits good response to NH₃ and NO₂ gas exposure. Moreover, the sensor maintains a good linearity between $\Delta R/R_0$ and the chemical gas concentration in logarithmic scale, 0.9978 to NH₃ and 0.9992 to NO₂, respectively. It indicates that the flexible SWNT sensor keeps its integrity and performance even under an applied stress.

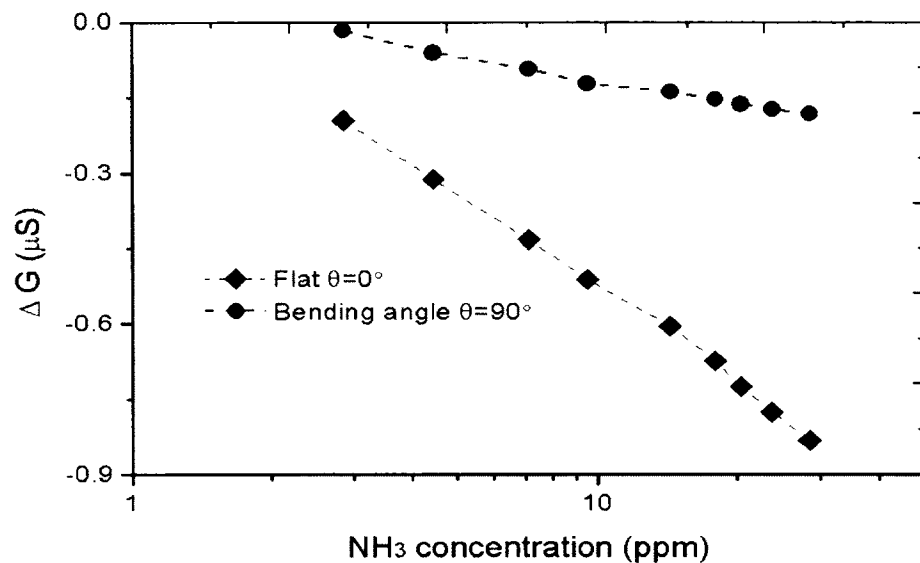


Figure 23. Comparison of the conductance change of the SWNT sensor with flat (bending angle 0°) and bent (bending angle 90°) substrate, when exposed to different NH₃ concentrations.

We also compared the conductance change ΔG of the SWNT sensor with flat (bending angle 0°) and bent (bending angle 90°) substrate. Figure 23 illustrates the conductance change with different bending angles when the sensor is exposed to different chemical concentrations of NH₃. Figure 23 and Figure 24 shows the plot of the conduct-

ance change exposed to NO_2 . The Drude conductivity relation shows the conductance of the CNT networks is proportional to $q\mu_p n_{CNT}$, where q is the electronic charge of the carrier, μ_p is hole mobility, and n_{CNT} is the carrier concentration in carbon nanotubes, which is tuned by the doping of chemical molecules adsorption. So the n_{CNT} is a function of the concentration of the chemical gas. The conductance change rate upon the chemical exposure is proportional to $q\mu_p$. The strain induced by the sensor bending may reduce the hole mobility [105], while q keeps constant. Therefore, the change rate decreases when bented at 90° compared with the one with flat substrate.

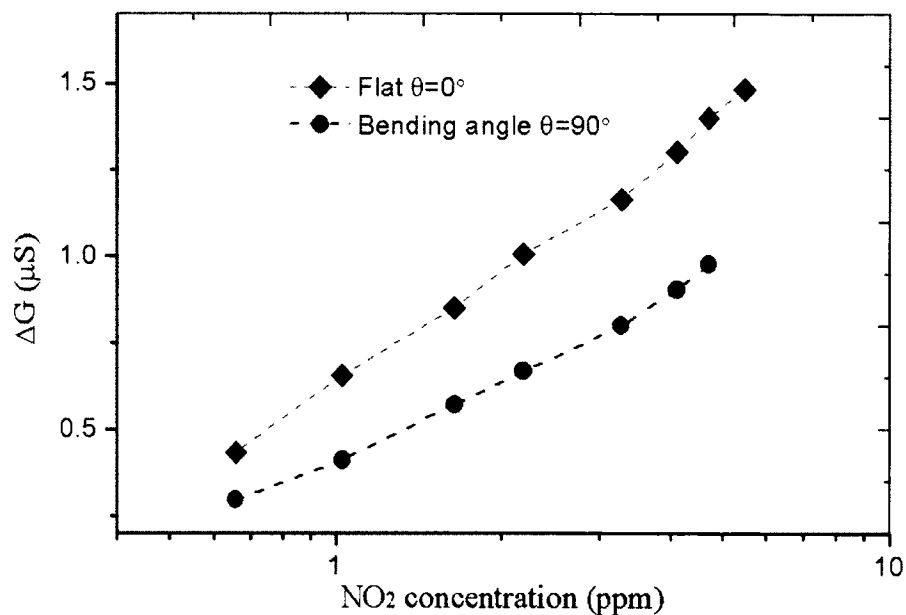


Figure 24. Comparison of the conductance change of the SWNT sensor with flat (bending angle 0°) and bent (bending angle 90°) substrate, when exposed to different NO_2 concentrations.

5 Conclusions

In this chapter, we report a high sensitive flexible SWNT chemical gas sensor, capable of being easily fabricated. High sensitivity, 1.32%/ppm for NH_3 detection, and

6.17%/ppm for NO₂ were obtained. The lowest detectable concentrations for NH₃ and NO₂ are 2.85 ppm and 659 ppb respectively.

The sensor also shows good performance in linearity and flexibility. In this chapter, we primarily have carried out experiment for sensing NH₃ and NO₂ with the flexible CNT sensor. In addition, the proposed sensor design has also been demonstrated applicable for other chemical gas sensing. Though some issues in terms of stability and selectivity still need be further investigated, the flexible printed SWNT sensor with high sensitivity, low LOD, and flexibility provides a promising solution to low-cost flexible sensor with high performance for mass production.

VI WIRELESS FLEXIBLE CNT GAS SENSOR

1 **Background**

Since discovered by Iijima [4], Carbon nanotubes have shown great promises in nano-electronics [6, 70, 106], transparent optical materials[107], actuators [108], and sensors [54, 88], particularly in flexible chemical gas sensors [109, 110], due to their excellent electronic and mechanical properties, such as mechanical flexibility [111], high electron mobility [68, 69], and high surface to volume ratio, etc. The high surface-to-volume ratio provides large surface areas for chemical absorption and thus offers high sensitivity for sensors, compared with other sensing materials.[112, 113] CNTs can also be purified and made into single-walled CNT suspension with high semiconducting SWNT concentration [70]. The SWNT suspension allows one to make dense SWNT networks on flexible or conformal surfaces through solution-casting or direct printing process. The printable high density SWNT networks with excellent mechanical flexibility are promising for the development of smart skins and wearable sensors with high sensitivity [114, 115].

In this chapter, we report a printable frequency-modulated passive wireless sensor tag based on the ultra-pure single-walled carbon nanotube networks with a high semiconducting SWNT concentration. The printable SWNT based NH₃ sensor shows an enhanced sensitivity of 0.76% per part per million (ppm) primarily due to the large surface area of the SWNT network. A high linearity is obtained between the resistance of the sensor and

the logarithm of the NH₃ concentration (referred to log [NH₃], hence forth). A simple frequency-modulated circuit including a ring oscillator, a rectifier, and a transmitting/receiving antenna is designed and fabricated to convert the resistance change to the oscillating frequency shift of the circuit. The wireless tag shows high linear response between the frequency shift and the log [NH₃] with a large frequency shift of 73.7 Hz/ppm. The linear response allows one to precisely predict the NH₃ concentration by measuring the frequency shift of the FM wireless sensor tag. Since the passive wireless sensor tag works in the FM-mode, noises due to the signal reflection and fluctuation can be greatly reduced. Such FM modulated passive wireless sensor tag with linear response and enhanced sensitivity is promising for power-less standalone low-level NH₃ sensing and monitoring with high accuracy.

2 Flexible Printable Sensor Fabrication

2.1 CNT Sensor Design

Figure 25 (a) shows the picture of the flexible SWNT ammonia sensor. It consists of a transparent flexible Kapton polyimide film as the substrate, a pair of inter-digit electrodes (IDEs), and a transparent layer of SWNT thin film coated on the top of the IDEs. Figure 25 (b) shows the close-up view of the flexible SWNT sensor. The width of the IDEs is 380 μm, the separation between two IDE fingers is 180 μm, and the length of the IDE is 1400 μm.

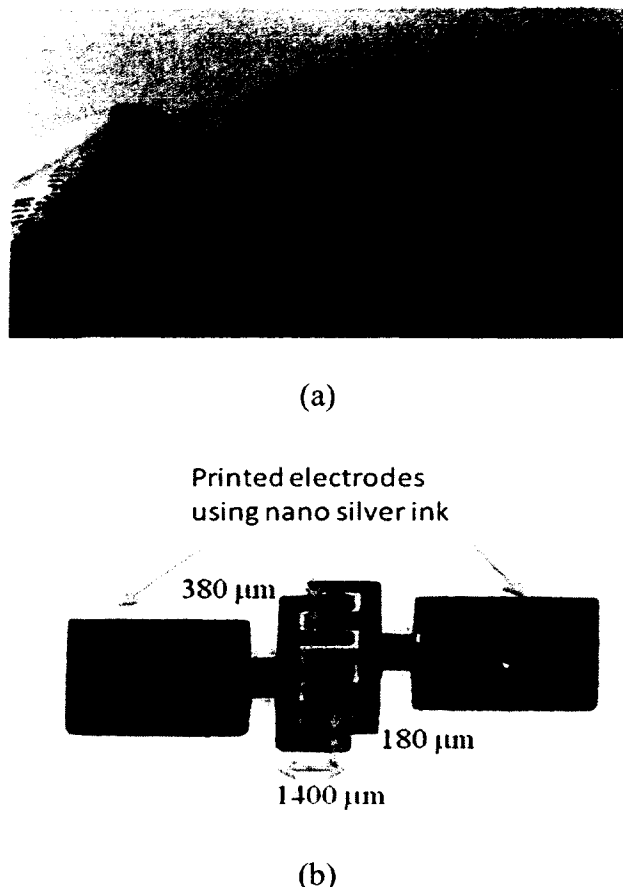


Figure 25. Flexible SWCNT based NH_3 sensor. (a) Picture of the sensor with IDEs and a transparent layer of SWCNT thin film on the top of the IDEs. (b) Close-up view of the flexible SWCNT sensor. The width of the IDEs is 380 μm , the separation between two IDE fingers is 180 μm , and the length of the IDE is 1400 μm .

The flexible SWNT sensor was fabricated following two major steps, i. e. IDE electrodes printing and the SWNT film deposition. First, UTDAg silver nanoink from UT-Dots were used to print the IDEs on a transparent flexible Kapton polyimide film using an Aerosol Jet® printing system from Optomec, Inc. The substrate and printed IDEs

were then heated at 130 °C for 30 mins for thermal annealing. Secondly, the SWNT film layer was deposited by drop-casting ultrapure SWNT dispersion (Brewer Science, Inc.) onto the flexible substrate with the printed IDEs. The ultrapure SWNT dispersion is water-based and surfactant-free containing less than 500 parts per billion (ppb) metal impurities in the dispersion. The SWNTs were functionalized with OH- groups to keep them dispersed and freely suspended in the solution.[57] In order to obtain an appropriate resistance value (1 to 2 kΩ) of the SWNT networks to make the wireless tag work properly, the flexible sensor was deposited by four times, forming four layers of SWNT films. Finally, the sensor device was placed on a hot plate at 90°C under atmosphere for 30 mins to improve the stability.

2.2 Characterization of the Flexible CNT Sensor

Before the flexible SWNT sensor was integrated into the wireless tag, the electrical characteristics of the device were measured using a dual source meter (2602, Keithley) in a sensor test chamber with a fixed environment temperature of 19.5°C. The sensor was initially purged with nitrogen (N₂) gas for 120 mins to stabilize the resistance of the sensor. Then, the sensor was exposed to the NH₃ flow with different concentrations for 20 mins until the resistance was stabilized. The sensor was purged by N₂ gas for 20 mins before each measurement. The resistance of the sensor was measured at each NH₃ concentration.

Figure 26 shows the curve of $\Delta R/R_0$ vs log [NH₃]. The resistance of the sensor increases with the concentration of the NH₃ gas. This is attributed to the electron donation from the NH₃ molecules to the SWNT networks when they are absorbed on the SWNT networks. The absorption and the electron donation process will not change the electronic

structures of the SWNTs [116]. Since the SWNT networks are primarily p-type semiconducting CNTs [76], the electron donation decreases the concentration of the p-type carriers and thus increases the resistance of the sensor. A good linear relationship is obtained between the resistance of the sensor and the log $[\text{NH}_3]$ within the measurement gas concentration range. The origin of the linear relationships is not clear and subject to further investigation. The linear response allows one to precisely predict the gas concentration by measuring the resistance of the sensor.

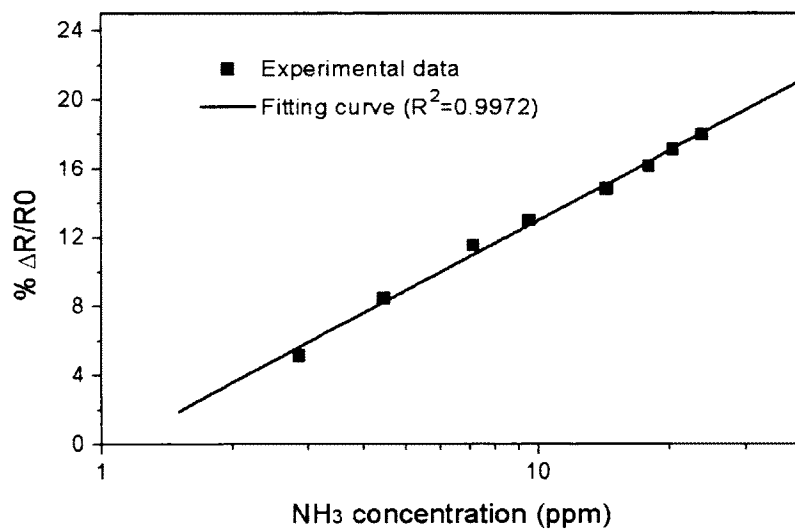


Figure 26. Relative resistance changes $\Delta R/R_0$ vs $\log [\text{NH}_3]$ curve. The resistance of the sensor increases with the concentration of the NH_3 gas due to the electron donation from the NH_3 molecules to the SWCNT networks. The squares are measurement data and the line is the linear fitting curve. A good linear relationship is obtained between the resistance of the sensor and the $\log [\text{NH}_3]$.

We define the sensor sensitivity as the relative resistance change per ppm as $S = (\Delta R/R_0)/\Delta \rho$, where $\Delta \rho$ is the concentration range of chemical gas molecules. A high

sensitivity of 0.76%/ppm is obtained for NH₃ at room temperature, which is much higher than other reported flexible ammonia sensors [117]. The sensor can also detect a low NH₃ concentration level of 2.85 ppm (lowest detection level (LDL) in the experiment). The high sensitivity and the low LDL are attributed to the high purity and dense SWNT networks with a large absorption area [7, 70, 76].

3 Wireless Sensor Design and Wireless Test System

3.1 Wireless Sensor Design

After testing the electrical properties of the flexible sensor, we designed a simple passive (battery-free) FM circuit and integrated the flexible sensor into the circuit. Figure 27 shows the schematic diagram of the passive FM wireless circuit. It consists of an RF antenna, a rectifier, a modulator, a ring oscillator, and the flexible SWNT gas sensor.

The antenna receives 13.56 MHz radio frequency (RF) signals from the sensor reader. The received RF signals are subsequently rectified by a bridge rectifier (D1-D4 in Fig. 3) to supply the power for the ring oscillator. A capacitor C1 is used to smooth the output voltage, and a parallel Zener diode (D5) regulates the voltage output. The ring oscillator consists of three digital inverters in a series feedback loop. Each inverter includes a single p-type MOSFET (ZXMD63P02X from Zetex) and two resistors. The three inverters are connected in series and form a positive feedback loop. The positive feedback plus the gain in the loop make the circuit oscillate automatically. The oscillation period of the ring oscillator is determined by the time of the signal to propagate through the whole loop, including the propagation time through the circuits and the time constant (RC) of the MOSFETs. The oscillation signal modulates the carrier signal of 13.56 MHz and gives the FM modulated signal. By varying the drain voltages applied on the MOSFETs

(M1-M3), one can change the capacitance of the MOSFETs and tune the RC time constants. In this way, the oscillation frequency of the circuit can be controlled by the applied voltages of the MOSFETs. Such MOSEFT based voltage-controlled oscillators (VCO) are common in passive (battery-free) RFID designs due to its low power consumption [118].

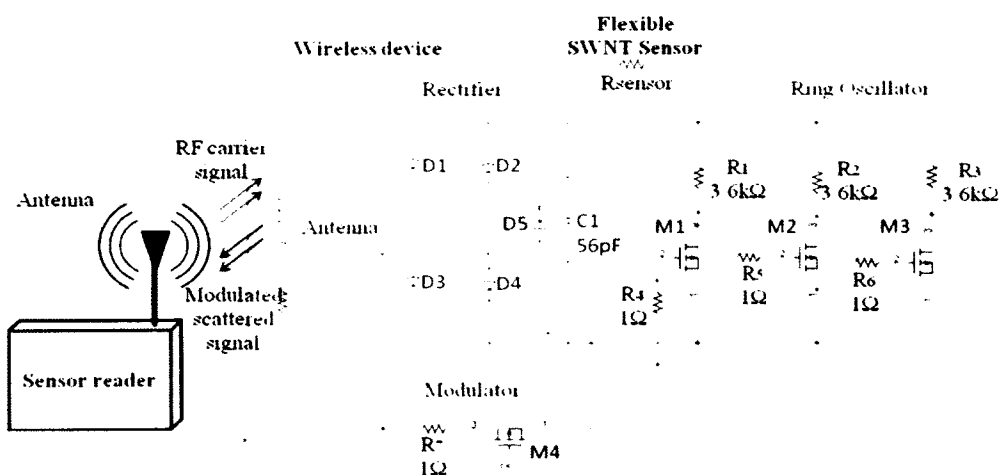


Figure 27. Circuit diagram of the passive FM wireless sensor tag. It consists of an RF antenna, a rectifier, a modulator, a ring oscillator, and the flexible SWNT gas sensor.

In this circuit, the voltage across the ring oscillator is tuned by varying the resistance of the flexible sensor through the exposure to the NH₃ gas. The absorption of NH₃ molecules changes the resistance of the sensor, which in turn modifies the voltages on the MOSFET and thus generates frequency shift of the oscillating frequency. The frequency-shifted output signal is then passed to the modulator (M4) where they are mixed with the 13.56 MHz RF signal and generates FM modulated signals. The FM modulated signals are finally transmitted back to the sensor reader (TRF7960 EVM Evaluation

Module, Texas Instruments) through the RF antenna. The FM modulated signals are received by the sensor reader and demodulated through the standard FM demodulation circuits. The frequency-shift signals are then retrieved and analyzed using a spectral analyzer.

3.2 Test System and Sensing Measurement

A test system for the wireless sensor measurement was designed and built to characterize the performance of the CNT wireless sensor. Figure 28 illustrates the diagram of the test system for the wireless device under different chemical gas concentrations. Nitrogen (N_2) gas is used as a carrier gas, and NH_3 as an analyte gas. The concentration of NH_3 is regulated by a gas generator (OVG4, Owlstone, UK) loaded with a NH_3 permeation tube (VICI Metronics). The OVG4 gas generator is controlled by the LabVIEW program. The device is placed into the sensor chamber, which is alternately purged by the N_2 gas with certain NH_3 concentration or the pure N_2 gas with a specific duration time by switching a 3-way valve. The sensor reader (TRF7960 EVM Evaluation Module, Texas Instruments) is placed outside the sensor chamber to test the wireless sensing capability of the device. A spectrum analyzer (N9912A, Agilent) is connected to the antenna on the sensor reader to measure the spectrum of the scattered signal from the wireless sensor device. The output waveform of the ring oscillation on the wireless sensor device is measured by an oscilloscope (DSO1024A, Agilent).

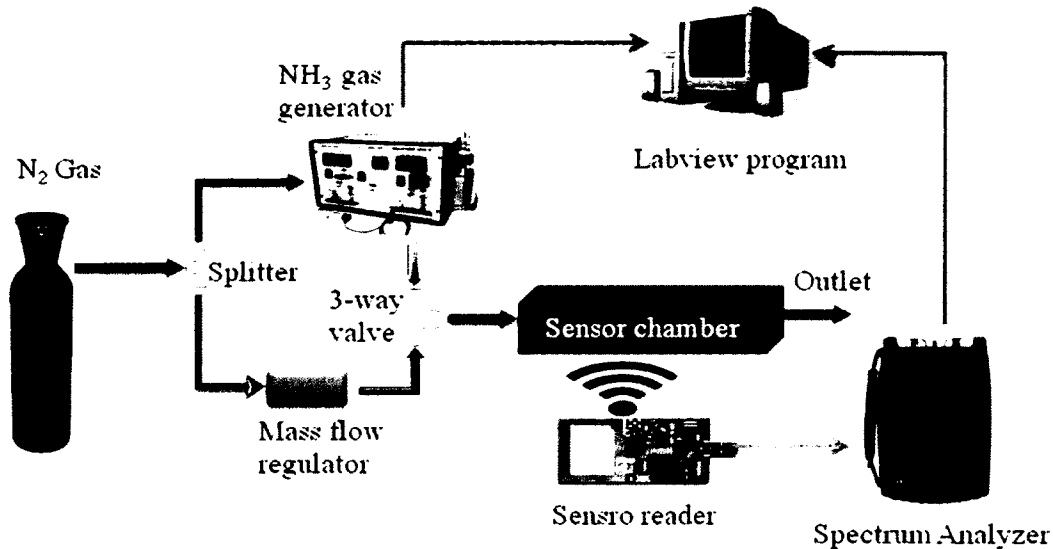


Figure 28. Diagram of the test system for the wireless device.

4 Results and Discussions

Figure 29 (a) illustrates the output waveforms of the ring oscillator exposed to different NH_3 concentration levels of ρ_{NH_3} of 2.85 ppm and 23.7 ppm, corresponding to the CNT sensor resistances of $R=1.45\text{ k}\Omega$ and $R=1.63\text{ k}\Omega$, respectively. The frequencies of the ring oscillator signals are 33.23 kHz and 31.97 kHz, respectively. Figure 29 (b) shows the spectra of the received signals by the sensor reader. The frequencies agree well with the output waveforms of the ring oscillator, indicating the effectiveness of the FM modulation and the wireless sensing configuration. The experiment also validates the accuracy of the NH_3 concentration level measurement by determining the frequency shift of the received signal in the reader.

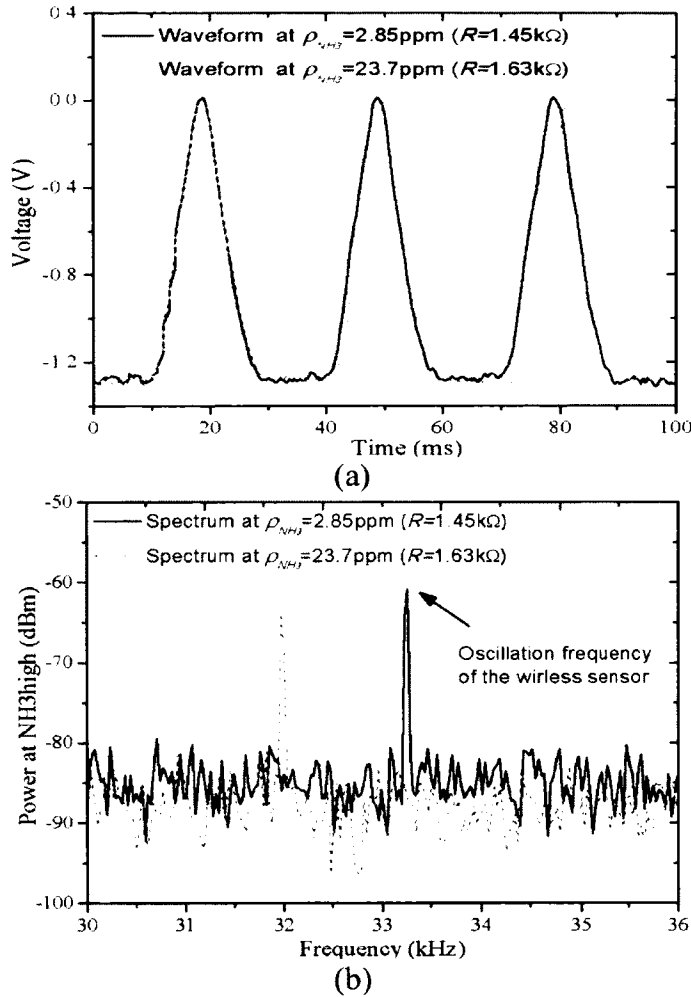


Figure 29. (a) Output waveforms of the ring oscillation of wireless sensor tag when exposed to different NH_3 concentration levels of NH_3 of 2.85 ppm and 23.7 ppm, corresponding to the CNT sensor resistances of $R=1.45\text{ k}\Omega$ and $R=1.63\text{ k}\Omega$, respectively. The frequencies of the ring oscillator signals are 33.23 kHz and 31.97 kHz, respectively. (b) Spectra of the received signals by the reader. The frequencies agree well with the output waveforms of the ring oscillator, indicating the effectiveness of the FM modulation and the wireless sensing configuration.

Figure 30 shows the plot of the oscillation frequencies vs the resistances of the CNT sensor. The wireless device exhibits a good linearity ($R^2=0.996$) between the sensor resistance and the oscillation frequency. Figure 31 illustrates the oscillation frequency dependence on the log $[\text{NH}_3]$. A good linear relation is obtained between the log $[\text{NH}_3]$ curve and the oscillation frequency with a linear correlation (R^2) of 0.988. The good linearity allows one to precisely predict the NH_3 concentration by measuring the frequency shift of the FM wireless sensor tag.

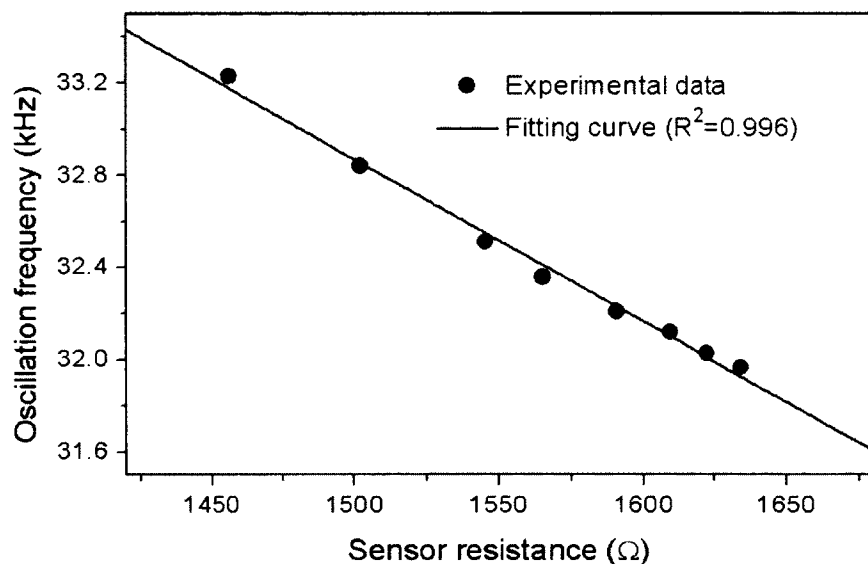


Figure 30 Linearity analysis of the wireless sensor tag. The circles and diamonds are the experimental data and the solid line is the linear fitting curve. Oscillation frequencies vs the resistances of the CNT sensor. A good linearity ($R^2=0.996$) is obtained between the sensor resistance and the oscillation frequency.

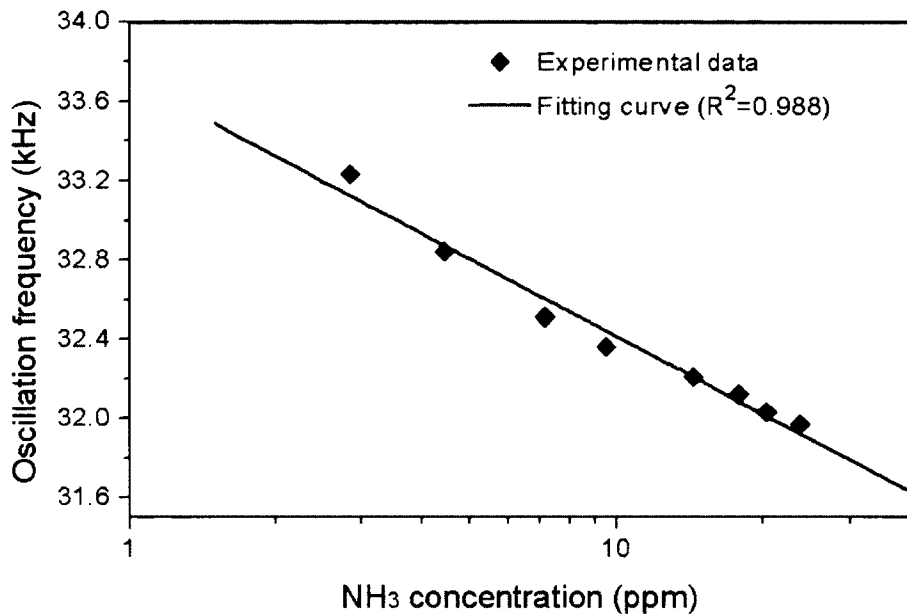


Figure 31. Linearity analysis of the wireless sensor tag. The circles and diamonds are the experimental data and the solid line is the linear fitting curve. Linear relation between the log [NH₃] curve and the oscillation frequency with a linear correlation (R^2) of 0.988.

5 Conclusions

We have developed a printable passive FM wireless sensor tag on a flexible substrate. The FM wireless sensor tag shows an enhanced sensitivity of 0.76%/ppm. The sensor tag also exhibits a high linearity between the frequency shift and the log [NH₃]. The linear response allows one to precisely predict the NH₃ concentration by measuring the frequency shift of the FM wireless sensor tag. In this chapter, we primarily have carried out experiment for wireless sensing for NH₃ molecules with the flexible CNT sensor. In addition, the proposed wireless CNT device has also been demonstrated applicable for other gas molecule sensing, such as NO₂, H₂O, etc.

In summary, the experimental demonstration of the passive wireless sensor tag and accurate measurement of the NH₃ concentration levels indicate that the FM modulated passive wireless sensor tag is promising for power-less standalone low-level NH₃ sensing and monitoring.

VII CONCLUSIONS

This dissertation conducts studies of SWNT electrical property models dependent upon the humidity and chemical gas concentration. The sensing mechanisms for different gas molecules are analyzed and compared. Furthermore, we investigate the CNT sensor applications, especially in flexible SWNT sensor and wireless CNT flexible sensors, which have wide and extensive applications in many aspects of our life, such as in public security, food quality control, industrial emission monitoring, and environmental pollution analysis.

1 Contributions

This dissertation made the following contributions:

- 1) The conductance of SWNT networks was investigated at different humidity level and device temperature. It is found that the conductance of SWNT networks is dominated by the thermal activation carrier hopping over the barriers between SWNTs. The average separation between SWNTs increases linearly with the humidity levels. The model of the humidity-dependent conductance of the SWNT network was proposed for the first time. The simulated results by the model were compared with the experimental data. The model agrees well with the experimental data. Such knowledge about the humidity effect on the electrical properties of CNT networks will not only benefit reliability studies of the CNT-based flexible elec-

tronics, but also facilitate the development of CNT-based humidity sensors with high sensitivity.

2) The electrical property model of SWNT networks with dependency upon chemical gas concentration (NH_3 and NO_2) has been investigated. The electrical response of SWNT networks of the sensor to gas flow with different chemical concentrations was characterized. The chemical gas concentration dependence of electrical property was investigated, and a conductance model of the CNT sensor was developed based on Langmuir adsorption isotherm for the first time. The model agrees well with the experimental data with high correlation coefficient. It was also found that the sensing mechanism is dominantly determined by charge transfer in this study. The primary objective of the sensor model of the electrical property is to understand the relationship between conductance of CNT networks and gas concentration. With this understanding, the model offers a measurement of gas concentration based upon the electrical property of CNT sensor.

3) We report a high sensitive flexible SWNT chemical gas sensor, capable of being easily fabricated. High sensitivity and low detectable concentrations for NH_3 and NO_2 were obtained. The sensor also shows good performance in linearity and flexibility. Though some issues in terms of stability and selectivity still need be further investigated, the flexible printed SWNT sensor with high sensitivity, low LOD, and flexibility provides a promising solution to low-cost flexible sensor with high performance for mass production.

4) We have developed a printable passive FM wireless sensor tag on a flexible substrate for ammonia detection. The FM wireless sensor tag shows an en-

hanced sensitivity of 0.76%/ppm. The sensor tag also exhibits a high linearity between the frequency shift and the logarithm of the chemical gas concentration. The linear response allows one to precisely predict the NH₃ concentration by measuring the frequency shift of the FM wireless sensor tag. The experimental demonstration of the accurate measurement of the NH₃ concentration levels indicate that the FM modulated passive wireless sensor tag is promising for power-less standalone low-level NH₃ sensing and monitoring. In addition, the proposed wireless CNT device has also been demonstrated applicable for other gas molecule sensing, such as NO₂, H₂O, etc.

2 Suggested Areas of Further Research

To extend the work presented in this dissertation, a few possible directions are suggested to be explored as following:

- 1) The absorption model of SWNT networks exposed to different gaseous chemical molecules needs to be studied. Langmuir adsorption isotherm and Freudlich adsorption isotherm should be compared and applied to the SWNT networks absorption to NH₃, NO₂, and other gaseous chemical molecules.
- 2) SWNT properties dependent on both chemical concentration and device temperature can be investigated, since the sensor performance is always affected by the environmental temperature in practical applications. We can study the chemical concentration and temperature dependence of the sheet conductance and contact resistance. The mathematical model of the electrical property can be derived based on the chemical concentration and device temperature.

3) We can study the energy level and change tendency of SWNT networks as a semiconducting material with different chemical concentration. The CNT sensing mechanism needs to be analyzed further.

3 Summary

In this dissertation, the SWNT electrical property dependency upon the humidity and chemical gas concentration was investigated. To exclude the effect from contact resistance, the sheet resistance of single-walled CNT networks was measured by transfer length method. The electrical response of SWNT networks of the sensor to different humidity level and chemical gas molecules (NH_3 and NO_2) at different concentration levels was measured. The gas concentration dependence of electrical property was investigated, and two electrical models of SWNT networks were developed based on carrier transportation and adsorption isotherm. The experimental data agrees well with models for different gas molecules. The primary objective of the sensor model is to understand the relationship between conductance of CNT networks and gas concentration. With this understanding, the model offers a measurement of gas concentration based upon the electrical property of CNT sensor. Furthermore, the mechanisms of gas molecule sensing on CNT networks were analyzed and compared with different gas molecules based on the models

In addition, the printed flexible electronic based on SWNTs and printable CNT-based FM passive wireless sensor tag on a flexible substrate with enhanced sensitivity are presented. Such FM modulated passive wireless sensor tag with linear response and enhanced sensitivity is promising for power-less standalone low-level NH_3 sensing and monitoring with high accuracy. The progress in these applications would contribute to

many aspects of our life, such as in public security, food quality control, industrial emission monitoring and control, environmental pollution analysis, and automotive industry.

VIII REFERENCES

1. Radushkevich, L. and V. Lukyanovich, *O strukture ugleroda, obrazujucegosja pri termiceskom razlozenii okisi ugleroda na zeleznom kontakte*. Zurn. Fisic. Chim., 1952. **26**: p. 88-95.
2. Balasubramanian, K. and M. Burghard, *Chemically Functionalized Carbon Nanotubes*. Small, 2005. **1**(2): p. 180-192.
3. Mahar, B., et al., *Development of Carbon Nanotube-Based Sensors: A Review*. Sensors Journal, IEEE, 2007. **7**(2): p. 266-284.
4. Iijima, S., *Helical Micro-tubules of Graphitic Carbon*. Nature, 1991. **345**: p. 56-58.
5. Collins, P.G. and P. Avouris, *Nanotubes for Electronics*. Scientific American, 2000. **283**(6): p. 62-69.
6. Cao, Q., et al., *Medium-scale carbon nanotube thin-film integrated circuits on flexible plastic substrates*. Nature, 2008. **454**(7203): p. 495-500.
7. Vaillancourt, J., et al., *All ink-jet-printed carbon nanotube thin-film transistor on a polyimide substrate with an ultrahigh operating frequency of over 5 GHz*. Applied Physics Letters, 2008. **93**(24): p. 243301.
8. Zhang, T. and et al., *Recent progress in carbon nanotube-based gas sensors*. Nanotechnology, 2008. **19**(33): p. 332001.
9. Ding, M., et al., *Chemical Sensing with Polyaniline Coated Single-Walled Carbon Nanotubes*. Advanced Materials, 2011. **23**(4): p. 536-540.
10. Du, K., et al., *Wafer-Scale Pattern Transfer of Metal Nanostructures on Polydimethylsiloxane (PDMS) Substrates via Holographic Nanopatterns*. ACS Applied Materials & Interfaces, 2012. **4**(10): p. 5505-5514.

11. Vasinajindakaw, P., et al., *A Fano-type interference enhanced quantum dot infrared photodetector*. Applied Physics Letters, 2011. **98**(21): p. 211111-211111-3.
12. Guo, J., et al., *Multi-walled carbon nanotubes coated by multi-layer silica for improving thermal conductivity of polymer composites*. Journal of Thermal Analysis and Calorimetry, 2013: p. 1-8.
13. Zou, X., et al. *Nondestructive characterization for PDMS thin films using a miniature fiber optic photoacoustic probe*. in *Proceedings of SPIE*, 8694. 2013. International Society for Optics and Photonics.
14. Li, Y., et al., *Poly (propylene)/Graphene Nanoplatelet Nanocomposites: Melt Rheological Behavior and Thermal, Electrical, and Electronic Properties*. Macromolecular Chemistry and Physics, 2011.
15. Li, Y., et al., *Poly (propylene) Nanocomposites Containing Various Carbon Nanostructures*. Macromolecular Chemistry and Physics, 2011. **212**(22): p. 2429-2438.
16. Zhu, J., et al., *Comprehensive and sustainable recycling of polymer nanocomposites*. J. Mater. Chem., 2011. **21**(40): p. 16239-16246.
17. Jiajie, D. and C. Guangde, *Optical properties of metal-coated nanoparticles*. Acta Photonica Sinica, 2001. **30**(5): p. 550-554.
18. El Mel, A.A., et al., *Highly Ordered Hollow Oxide Nanostructures: The Kirkendall Effect at the Nanoscale*. Small, 2013: p. n/a-n/a.
19. Mao, A., C.D. Schaper, and R.F.K. Jr, *Nanopatterning using a simple bi-layer lift-off process for the fabrication of a photonic crystal nanostructure*. Nanotechnology, 2013. **24**(8): p. 085302.
20. Diao, J., et al., *Surface vertical deposition for gold nanoparticle film*. Journal of Physics D: Applied Physics, 2003. **36**(3): p. L25.
21. Wei, H., et al., *Electrochromic Poly (DNTD)/WO₃ Nanocomposite Films via Electropolymerization*. The Journal of Physical Chemistry C, 2012. **116**(30): p. 16286-16293.

22. Li, Y. and S. Zhou, *A simple method to fabricate fluorescent glucose sensor based on dye-complexed microgels.* Sensors and Actuators B: Chemical, 2013. **177**(0): p. 792-799.
23. Yu, Z., et al., *Selective Tumor Cell Targeting by the Disaccharide Moiety of Bleomycin.* Journal of the American Chemical Society, 2013. **135**(8): p. 2883-2886.
24. Yu, Z., et al., *Selective and facile assay of human immunodeficiency virus protease activity by a novel fluorogenic reaction.* Analytical Biochemistry, 2010. **397**(2): p. 197-201.
25. Tonooka, K., et al., *Facile Assay of Telomerase Activity Utilizing a DNA-detectable Chemiluminogenic Reagent.* Analytical Sciences, 2008. **24**(4): p. 471-475.
26. Diao, J. and Q. Cao, *Gold nanoparticle wire and integrated wire array for electronic detection of chemical and biological molecules.* AIP Advances, 2011. **1**: p. pp. 012115-5.
27. Diao, J., et al., *Nanoparticle delivery by controlled bacteria.* Journal of nanoscience and nanotechnology, 2005. **5**(10): p. 1749-1751.
28. Ling, Y., et al., *Thin film thickness variation measurement using dual LEDs and reflectometric interference spectroscopy model in biosensor.* 2010: p. 75590K-75590K.
29. Tian, Y., H.-j. Wang, and Z.-l. Fang, *The pupil diameter precise measurement based on morphological reconstruction algorithm.* Journal of Optoelectronics Laser, 2008. **19**(3): p. 409.
30. Tian, Y. and X. Wang. *In-vivo blood pressure measurements using a miniature fiber optic sensor with special packaging for diagnosis of coronary artery disease.* in *BIT's 2nd Annual Conference and EXPO of AnalytiX: Biosensor and Application.* 2013.
31. Hu, Y., et al., *A highly selective chemical sensor array based on nanowire/nanostructure for gas identification.* Sensors and Actuators B: Chemical, 2013. **181**(0): p. 424-431.

32. Ding, M., et al., *Welding of Gold Nanoparticles on Graphitic Templates for Chemical Sensing*. Journal of the American Chemical Society, 2012. **134**(7): p. 3472-3479.
33. Yushi, H., et al., *A Single Palladium Nanowire Via Electrophoresis Deposition Used as a Ultrasensitive Hydrogen Sensor*. Nanotechnology, IEEE Transactions on, 2008. **7**(6): p. 693-699.
34. Wang, Q., Y. Liu, and X. Pan, *Atmosphere pollutants and mortality rate of respiratory diseases in Beijing*. Science of The Total Environment, 2008. **391**(1): p. 143-148.
35. Wu, N., et al., *Label-free detection of biomolecules using LED technology*. 2010: p. 75740I-75740I.
36. Tian, Y., et al., *Tapered optical fiber sensor for label-free detection of biomolecules*. Sensors, 2011. **11**(4): p. 3780-3790.
37. Tian, Y., et al., *Label-free detection of biomolecules using a tapered optical fiber sensor*. Proceedings of SPIE, 2010. **7673**: p. 767307.
38. Ling, Y., et al., *A printable CNT-based FM passive wireless sensor tag on a flexible substrate with enhanced sensitivity*. Sensors Journal, IEEE (Submitted), 2013. (): p. .
39. Monthioux, M. and V.L. Kuznetsov, *Who should be given the credit for the discovery of carbon nanotubes?* Carbon, 2006. **44**(9): p. 1621-1623.
40. Iijima, S. and T. Ichihashi, *Single-shell carbon nanotubes of 1-nm diameter*. Nature, 1993. **363**(6430): p. 603-605.
41. Bethune, D.S., et al., *Cobalt-catalysed growth of carbon nanotubes with single-atomic-layer walls*. Nature, 1993. **363**: p. 605-607.
42. Tang, X., et al., *Carbon Nanotube DNA Sensor and Sensing Mechanism*. Nano Letters, 2006. **6**(8): p. 1632-1636.
43. Chang, H., et al., *Adsorption of NH₃ and NO₂ molecules on carbon nanotubes*. Applied Physics Letters, 2001. **79**(23): p. 3863-3865.
44. Kong, J., et al., *Nanotube Molecular Wires as Chemical Sensors*. Science, 2000. **287**(5453): p. 622-625.

45. Odom, T.W., et al., *Atomic structure and electronic properties of single-walled carbon nanotubes*. Nature, 1998. **391**(6662): p. 62-64.
46. Wilder, J.W., et al., *Electronic structure of atomically resolved carbon nanotubes*. Nature, 1998. **391**(6662): p. 59-62.
47. Treacy, M.M.J., T.W. Ebbesen, and J.M. Gibson, *Exceptionally high Young's modulus observed for individual carbon nanotubes*. Nature, 1996. **381**(6584): p. 678-680.
48. Yu, M.-F., et al., *Tensile Loading of Ropes of Single Wall Carbon Nanotubes and their Mechanical Properties*. Physical Review Letters, 2000. **84**(24): p. 5552-5555.
49. Quang, N.H., et al., *Effect of NH₃ gas on the electrical properties of single-walled carbon nanotube bundles*. Sensors and Actuators B: Chemical, 2006. **113**(1): p. 341-346.
50. Junya, S. and et al., *Fabrication of a carbon nanotube-based gas sensor using dielectrophoresis and its application for ammonia detection by impedance spectroscopy*. Journal of Physics D: Applied Physics, 2003. **36**(21): p. L109.
51. Cantalini, C., et al., *Sensitivity to NO₂ and cross-sensitivity analysis to NH₃, ethanol and humidity of carbon nanotubes thin film prepared by PECVD*. Sensors and Actuators B: Chemical, 2003. **95**(1-3): p. 195-202.
52. Liu, L., et al., *Humidity Sensitivity of Multi-Walled Carbon Nanotube Networks Deposited by Dielectrophoresis*. Sensors, 2009. **9**(3): p. 1714-1721.
53. Ding, M., D.C. Sorescu, and A. Star, *Photoinduced Charge Transfer and Acetone Sensitivity of Single-Walled Carbon Nanotube-Titanium Dioxide Hybrids*. Journal of the American Chemical Society, 2013.
54. Fadel, T.R., et al., *Enhanced Cellular Activation with Single Walled Carbon Nanotube Bundles Presenting Antibody Stimuli*. Nano Letters, 2008. **8**(7): p. 2070-2076.
55. Bekyarova, E., et al., *Mechanism of Ammonia Detection by Chemically Functionalized Single-Walled Carbon Nanotubes: In Situ Electrical and Optical Study of Gas Analyte Detection*. Journal of the American Chemical Society, 2007. **129**(35): p. 10700-10706.

56. Yoon, H., et al., *Passive wireless sensors using electrical transition of carbon nanotube junctions in polymer matrix*. Smart Materials and Structures, 2006. **15**(1): p. S14.
57. Ling, Y., et al., *Investigation of the Humidity-Dependent Conductance of Single-Walled Carbon Nanotube Networks*. Journal of Applied Physics, 2012.
58. Goldoni, A., et al., *Sensing gases with carbon nanotubes: a review of the actual situation*. Journal of Physics: Condensed Matter, 2010. **22**(1): p. 013001.
59. Derycke, V., et al., *Controlling doping and carrier injection in carbon nanotube transistors*. Applied Physics Letters, 2002. **80**(15): p. 2773-2775.
60. Mao, D., et al., *Polarization behavior of poly(vinylidene fluoride-trifluoroethylene) copolymer ferroelectric thin film capacitors for nonvolatile memory application in flexible electronics*. Journal of Applied Physics, 2010. **108**(9): p. 094102.
61. Mao, D., et al., *Fatigue characteristics of poly(vinylidene fluoride-trifluoroethylene) copolymer ferroelectric thin film capacitors for flexible electronics memory applications*. Organic Electronics, 2011. **12**(8): p. 1298-1303.
62. Kuang, Q., et al., *High-Sensitivity Humidity Sensor Based on a Single SnO₂ Nanowire*. Journal of the American Chemical Society, 2007. **129**(19): p. 6070-6071.
63. Yeow, J. and J. She, *Carbon nanotube-enhanced capillary condensation for a capacitive humidity sensor*. Nanotechnology, 2006. **17**(21): p. 5441.
64. Li, J., et al., *Carbon nanotube sensors for gas and organic vapor detection*. Nano Letters, 2003. **3**(7): p. 929-933.
65. Ahmad, M.M., S.A. Makhlof, and K.M.S. Khalil, *Dielectric behavior and ac conductivity study of NiO/Al₂O₃ nanocomposites in humid atmosphere*. Journal of Applied Physics, 2006. **100**(9): p. 094323.
66. Kim, S.J., et al., *Humidity sensors using porous silicon layer with mesa structure*. Journal of Physics D: Applied Physics, 2000. **33**(15): p. 1781.
67. Madden, J.D.W., *Stiffer Than Steel*. Science, 2009. **323**(5921): p. 1571-1572.
68. Dürkop, T., et al., *Extraordinary Mobility in Semiconducting Carbon Nanotubes*. Nano Letters, 2004. **4**(1): p. 35-39.

69. Bradley, K., J.-C.P. Gabriel, and G. Grüner, *Flexible Nanotube Electronics*. Nano Letters, 2003. **3**(10): p. 1353-1355.
70. Gu, G., et al., *All-Printed Thin-Film Transistor Based on Purified Single-Walled Carbon Nanotubes with Linear Response*. Journal of Nanotechnology, 2011.
71. Liu, L., et al., *Humidity Sensitivity of Carbon Nanotube and Poly(Dimethyldiallyl ammonium Chloride) Composite Films*. Sensors Journal, IEEE, 2009. **9**(10): p. 1308-1314.
72. Pati, R., et al., *Effect of H₂O adsorption on electron transport in a carbon nanotube*. Applied Physics Letters, 2002. **81**(14): p. 2638-2640.
73. Tang, Q., Y.C. Chan, and K. Zhang, *Fast response resistive humidity sensitivity of polyimide/multiwall carbon nanotube composite films*. Sensors and Actuators B: Chemical, 2011. **152**(1): p. 99-106.
74. Vaillancourt, J., et al., *High-speed thin-film transistor on flexible substrate fabricated at room temperature*. Electronics Letters, 2006. **42**(23): p. 1365-1367.
75. Han, X., et al., *Printable high-speed thin-film transistor on flexible substrate using carbon nanotube solution*. Micro & Nano Letters, 2007. **2**(4): p. 96-98.
76. Gu, G., et al. *All-printed CNT transistors with high on-off ratio and bias-invariant transconductance*. in *Proceedings of the SPIE*. 2011.
77. Kaiser, A.B., *Electronic transport properties of conducting polymers and carbon nanotubes*. Reports on Progress in Physics, 2001. **64**(1): p. 1.
78. Zhang, H., et al., *Electrical and thermal properties of carbon nanotube bulk materials: Experimental studies for the 328-958 K temperature range*. Physical Review B, 2007. **75**(20): p. 205407.
79. Koechlin, C., et al., *Electrical characterization of devices based on carbon nanotube films*. Vol. 96. 2010: AIP. 103501.
80. Mott, N.F. and E.A. Davis, *Electronic processes in non-crystalline materials* 1971: Clarendon Press.
81. Sheng, P., *Fluctuation-induced tunneling conduction in disordered materials*. Physical Review B, 1980. **21**(6): p. 2180.
82. Jackson, R. and S. Graham, *Specific contact resistance at metal/carbon nanotube interfaces*. Appl. Phys. Lett., 2009. **94**: p. 012109.

83. Loh, W.M., et al., *Modeling and measurement of contact resistances*. Electron Devices, IEEE Transactions on, 1987. **34**(3): p. 512-524.
84. Berger, H.H., *Contact Resistance and Contact Resistivity*. Journal of the Electrochemical Society, 1972. **119**(4): p. 507-514.
85. Peng, S. and K. Cho, *Chemical control of nanotube electronics*. Nanotechnology, 2000. **11**(2): p. 57.
86. Peng, N., et al., *Sensing Mechanisms for Carbon Nanotube Based NH₃ Gas Detection*. Nano Letters, 2009. **9**(4): p. 1626-1630.
87. (ATSDR), A.f.T.S.a.D.R., *Toxic FAQ Sheet for Ammonia*. 2004.
88. Ting, Z., et al., *Poly(m-aminobenzene sulfonic acid) functionalized single-walled carbon nanotubes based gas sensor*. Nanotechnology, 2007. **18**(16): p. 165504.
89. Varghese, O.K., et al., *Gas sensing characteristics of multi-wall carbon nanotubes*. Sensors and Actuators B: Chemical, 2001. **81**(1): p. 32-41.
90. Wang, C., et al., *Wafer-Scale Fabrication of Separated Carbon Nanotube Thin-Film Transistors for Display Applications*. Nano Letters, 2009. **9**(12): p. 4285-4291.
91. Ling, Y., et al., *Investigation of the humidity-dependent conductance of single-walled carbon nanotube networks*. Journal of Applied Physics, 2013. **113**(2): p. 024312.
92. Marulanda, J.M. and A. Srivastava, *Carrier density and effective mass calculations in carbon nanotubes*. physica status solidi (b), 2008. **245**(11): p. 2558-2562.
93. Fuhrer, M.S., et al., *High-Mobility Nanotube Transistor Memory*. Nano Letters, 2002. **2**(7): p. 755-759.
94. Ammu, S., et al., *Flexible, All-Organic Chemiresistor for Detecting Chemically Aggressive Vapors*. Journal of the American Chemical Society, 2012. **134**(10): p. 4553-4556.
95. Mao, D., et al., *Optimization of poly(vinylidene fluoride-trifluoroethylene) films as non-volatile memory for flexible electronics*. Organic Electronics, 2010. **11**(5): p. 925-932.

96. Gu, G., et al. *All-printed CNT transistors with high on-off ratio and bias-invariant transconductance*. in *Proc. SPIE*. 2011.
97. Vaillancourt, J., et al., *All ink-jet-printed carbon nanotube thin-film transistor on a polyimide substrate with an ultrahigh operating frequency of over 5 GHz*. *Appl. Phys. Lett.*, 2008. **93**(24): p. 243301.
98. Ammu, S., et al., *Flexible, All-Organic Chemiresistor for Detecting Chemically Aggressive Vapors*. *J. Am. Chem. Soc.*, 2012. **134**(10): p. 4553-4556.
99. Yang, L., et al., *A Novel Conformal RFID-Enabled Module Utilizing Inkjet-Printed Antennas and Carbon Nanotubes for Gas-Detection Applications*. *IEEE Antenn. Wireless Propag. Lett.*, 2009. **8**: p. 653-656.
100. Fu, D., et al., *Differentiation of Gas Molecules Using Flexible and All-Carbon Nanotube Devices*. *J. Phys. Chem. C*, 2008. **112**(3): p. 650-653.
101. Gu, G., et al., *All-Printed Thin-Film Transistor Based on Purified Single-Walled Carbon Nanotubes with Linear Response*. *J. Nanotech.*, 2011. **2011**.
102. Yang, L., et al., *Band-gap change of carbon nanotubes: Effect of small uniaxial and torsional strain*. *Physical Review B*, 1999. **60**(19): p. 13874-13878.
103. Shimamura, Y., Y. Tetsuo, and A. Todoroki, *Strain Sensing by Using Piezoresistivity of Carbon-Nanotube/Flexible-Epoxy Composite* in *Proc. 16th International Conference on Composite Materials* 2007 p. 1198-1199.
104. Hu, N., et al., *Tunneling effect in a polymer/carbon nanotube nanocomposite strain sensor*. *Acta Materialia*, 2008. **56**(13): p. 2929-2936.
105. Sreekala, S., et al., *Effect of strain on the band gap and effective mass of zigzag single-wall carbon nanotubes: First-principles density-functional calculations*. *Physical Review B*, 2008. **77**(15): p. 155434.
106. Selvarasah, S., et al. *A Novel Three Dimensional Field Effect Transistor Based on Single-Walled Carbon Nanotubes*. in *Nanotechnology, 2008. NANO '08. 8th IEEE Conference on*. 2008.
107. Wu, Z., et al., *Transparent, Conductive Carbon Nanotube Films*. *Science*, 2004. **305**(5688): p. 1273-1276.
108. Madden, J.D.W., et al., *Fast Carbon Nanotube Charging and Actuation*. *Advanced Materials*, 2006. **18**(7): p. 870-873.

109. Sun, X. and Y. Sun, *Single-Walled Carbon Nanotubes for Flexible Electronics and Sensors*. J. Mater. Sci. Technol., 2008. **24**(04): p. 569-577.
110. Parikh, K., et al., *Flexible vapour sensors using single walled carbon nanotubes*. Sensors and Actuators B: Chemical, 2006. **113**(1): p. 55-63.
111. Peng, H., *Aligned Carbon Nanotube/Polymer Composite Films with Robust Flexibility, High Transparency, and Excellent Conductivity*. Journal of the American Chemical Society, 2007. **130**(1): p. 42-43.
112. Yushi, H., et al. *Single metal and conducting polymer nanowires used as chemical/bio molecular sensors*. in *Nanotechnology (IEEE-NANO), 2010 10th IEEE Conference on*. 2010.
113. Kauffman, D.R. and A. Star, *Carbon Nanotube Gas and Vapor Sensors*. Angewandte Chemie International Edition, 2008. **47**(35): p. 6550-6570.
114. Kang, I., et al., *Introduction to carbon nanotube and nanofiber smart materials*. Composites Part B: Engineering, 2006. **37**(6): p. 382-394.
115. Abraham, J.K., et al., *Carbon nanotube strain sensors for wearable patient monitoring applications*. 2008: p. 69310J-69310J.
116. Loh, K.J., J.P. Lynch, and N.A. Kotov, *Passive wireless sensing using SWNT-based multifunctional thin film patches*. International Journal of Applied Electromagnetics & Mechanics, 2008. **28**(1/2): p. 87-94.
117. Yang, L., et al., *A Novel Conformal RFID-Enabled Module Utilizing Inkjet-Printed Antennas and Carbon Nanotubes for Gas-Detection Applications*. Antennas and Wireless Propagation Letters, IEEE, 2009. **8**: p. 653-656.
118. Klapf, C., et al. *Analyses and design of low power clock generators for RFID TAGs*. in *Research in Microelectronics and Electronics, 2008. PRIME 2008. Ph.D.* 2008.